JEM Journal of Experimental Medicine

ARTICLE

Inhibition of $GABA_A$ receptors in intestinal stem cells prevents chemoradiotherapy-induced intestinal toxicity

Cuiyu Zhang[1], Yuping Zhou[2], Junjie Zheng[1], Nannan Ning[3], Haining Liu[4], Wenyang Jiang[5], Xin Yu[6], Kun Mu[7], Yan Li[8], Wei Guo[9], Huili Hu[10], Jingxin Li[1], and Dawei Chen[1,11]

Lethal intestinal tissue toxicity is a common side effect and a dose-limiting factor in chemoradiotherapy. Chemoradiotherapy can trigger DNA damage and induce P53-dependent apoptosis in LGR5⁺ intestinal stem cells (ISCs). Gamma-aminobutyric acid (GABA) and its A receptors ($GABA_AR$) are present in the gastrointestinal tract. However, the functioning of the GABAergic system in ISCs is poorly defined. We found that $GABA_AR$ α1 (GABRA1) levels increased in the murine intestine after chemoradiotherapy. GABRA1 depletion in LGR5⁺ ISCs protected the intestine from chemoradiotherapy-induced P53-dependent apoptosis and prolonged animal survival. The administration of bicuculline, a $GABA_AR$ antagonist, prevented chemoradiotherapy-induced ISC loss and intestinal damage without reducing the chemoradiosensitivity of tumors. Mechanistically, it was associated with the reduction of reactive oxygen species–induced DNA damage via the L-type voltage-dependent Ca^{2+} channels. Notably, flumazenil, a $GABA_AR$ antagonist approved by the U.S. Food and Drug Administration, rescued human colonic organoids from chemoradiotherapy-induced toxicity. Therefore, flumazenil may be a promising drug for reducing the gastrointestinal side effects of chemoradiotherapy.

Introduction

The intestine is a radiosensitive organ due to the rapid proliferation of intestinal stem cells (ISCs). Leucine-rich repeats containing G protein–coupled receptor 5 (LGR5)–positive ISCs or crypt base columnar cells, which are located at the base of crypts, can differentiate into various mature intestinal epithelial cells (IECs) and mediate repair after injury (Yu, 2013). The loss of LGR5⁺ ISCs is associated with DNA damage–dependent apoptosis caused by chemoradiotherapy (Keefe et al., 2000; Liu et al., 2016). One of the earliest reactions after DNA damage is the phosphorylation of the C-terminal serine residue of histone H2AX (Siddiqui et al., 2015). In eukaryotes, the phosphorylation of histone H2AX is mediated by members of the PIKKs family, including ataxia telangiectasia mutated (ATM), ATM and RAD3-related protein, and DNA-dependent protein kinase (Guleria and Chandna, 2016). Phosphorylated γ-H2AX quickly transduces DNA damage signals, leading to the activation of the phosphorylation of downstream molecules, e.g., P53 (Mirzayans et al., 2012). Activation of P53 after DNA damage can result in acute toxicity and accounts for most chemoradiotherapy-induced apoptosis and acute loss of ISCs (Leibowitz et al., 2018; Qiu et al., 2010). Therefore, inhibition of γ-H2AX or P53-dependent apoptosis is likely to alleviate the loss of stem cells caused by chemoradiotherapy.

γ-Aminobutyric acid (GABA) is an amino acid that acts as a major inhibitory neurotransmitter between nerve cells in the central nervous system (Roberts and Frankel, 1950). It is mainly synthesized from glutamate and catalyzed by glutamate decarboxylase (GAD). GAD has two isomers: GAD65 and GAD67. GABA

[1]Department of Physiology, School of Basic Medical Sciences, Qilu Hospital, Cheeloo College of Medicine, Shandong University, Jinan, Shandong, China; [2]Department of Cardiology, State Key Laboratory of Complex Severe and Rare Diseases, Peking Union Medical College Hospital, Chinese Academy of Medical Sciences and Peking Union Medical College, Beijing, China; [3]Department of Clinical Laboratory, Qilu Hospital, Cheeloo College of Medicine, Shandong University, Jinan, Shandong, China; [4]Department of Liver Surgery, The First Affiliated Hospital, Sun Yat-sen University, Guangzhou, Guangdong, China; [5]State Key Laboratory of Cardiovascular Disease, Fuwai Hospital, National Center for Cardiovascular Disease, Chinese Academy of Medical Sciences, Peking Union Medical College, Beijing, China; [6]Department of Biotherapy, State Key laboratory of Biotherapy and cancer center, West China Hospital, Sichuan University, Chengdu, Sichuan, China; [7]Department of Pathology, Qilu Hospital, Cheeloo College of Medicine, Shandong University, Jinan, Shandong, China; [8]Translational Medical Research Center, The First Affiliated Hospital of Shandong First Medical University and Shandong Provincial Qianfoshan Hospital, Jinan, Shandong, China; [9]Department of Colorectal Surgery, Qilu Hospital, Cheeloo College of Medicine, Shandong University, Jinan, Shandong, China; [10]Department of Systems Biomedicine and Research Center of Stem Cell and Regenerative Medicine, Shandong University Cheeloo Medical College, School of Basic Medical Sciences, Jinan, China; [11]Laboratory of Medical Chemistry, GIGA-Stem Cells, Faculty of Medicine, University of Liège, CHU, Sart-Tilman, Liège, Belgium.

Correspondence to Dawei Chen: dawei.chen@uliege.be; Jingxin Li: ljingxin@sdu.edu.cn.

is degraded by GABA-transaminase. The high-affinity sodium-dependent GABA transporter (GAT) is involved in controlling the concentration of extracellular GABA. GAT includes four subtypes: GAT1, GAT2, GAT3, and GAT4, of which GAT1 and GAT3 are the most common (Roth and Draguhn, 2012). $GABA_A$ receptors ($GABA_AR$) are ionotropic chloride channels composed of a combination of different subunits, including α (1–6), β (1–3), γ (1–3), δ, ε, θ, π, and ρ (Olsen and Sieghart, 2008). Apart from its well-known role in the mature central nervous system (Liu et al., 2005), the GABAergic system is also present in various peripheral tissues, such as the gastrointestinal tract (Auteri et al., 2015) and liver (Erlitzki et al., 2000). GABA signaling has a significant impact on the regulation of intestinal function. Previous studies have shown that early life stress-induced colonic inflammation is mediated by $GABA_AR$ in mice (Seifi et al., 2018). In addition, blocking $GABA_AR$ alleviates dextran sulfate sodium–induced experimental colitis (Ma et al., 2018).

Here, we sought to determine the role of the GABAergic signaling system in chemoradiotherapy-induced IEC death. We found that the depletion of $GABA_AR$ α1 (GABRA1) in $LGR5^+$ ISCs and the treatment with the $GABA_AR$ antagonist bicuculline provide effective protection against 5-fluorouracil (5-FU)– or irradiation-induced P53-dependent apoptosis in nonmalignant intestinal epithelium, while having no effect on tumor treatment in vivo. Further analysis showed that this protection relies on the reduction of ROS-induced DNA damage via L-type voltage-dependent Ca^{2+} channels. In addition, we proved that flumazenil, another $GABA_AR$ antagonist that has already been approved by the United States Food and Drug Administration (FDA), potently alleviated intestinal damage induced by chemoradiotherapy. Our findings provide new insights into the role of $GABA_AR$ antagonists in intestinal chemoradioprotection by selectively reducing ROS-induced apoptosis of $LGR5^+$ ISCs.

Results

$GABA_AR$ α1 was upregulated in mouse small intestinal crypts after 5-FU or irradiation treatment

We found that the transcription level of *Gabra1* in mouse intestinal tissues showed an upward trend after 5-FU (Fig. 1 A) or irradiation treatment (Fig. 1 B). Additionally, GABRA1 staining showed that it was significantly upregulated in crypts following 5-FU or irradiation treatment (Fig. 1 C). Western blot analysis showed that GABRA1 protein levels increased in the mouse intestinal crypts after 5-FU (Fig. 1 D) or irradiation treatment (Fig. 1 E).

Subsequently, immunohistochemistry staining showed that GAD65/67 was widely expressed in IECs, especially in crypts (Fig. 1 F). The expression areas of GABRA1 were similar to those of GAD65/67, and the expression level gradually increased along the villi–crypt axis (Fig. 1 F). Immunofluorescence showed that GABRA1 was expressed in $LGR5^+$ ISCs (Fig. 1 G). We also found that GAD65/67 and GABRA1 were expressed in human intestinal crypts (Fig. 1 H).

Taken together, these findings demonstrate that GAD65/67 and GABRA1 are widely expressed in mouse and human small intestinal crypts, and GABRA1 is upregulated in mouse intestinal crypts after 5-FU or irradiation treatment, indicating that the GABAergic system may be involved in chemoradiotherapy-induced intestinal toxicity.

Loss of *Gabra1* in IECs had no effect on the physiological phenotype of the intestine in mice

To investigate the potential role of GABRA1 in IECs under homeostatic conditions, we crossed *Villin-Cre* mice with $Gabra1^{flox/flox}$ mice to specifically knock out *Gabra1* in IECs ($Gabra1^{IEC\text{-}KO}$). The villus length (Fig. S1 A) and various epithelial cells, including goblet cells (Fig. S1 B), Paneth cells (Fig. S1 C), transit-amplifying cells (TACs; Fig. S1 D), BrdU-positive cells (Fig. S1 E), and olfactomedin 4 (OLFM4)–positive ISCs (Fig. S1 F) were examined; however, no noticeable change was observed after GABRA1 deletion. Collectively, these data suggest that the loss of *Gabra1* in IECs had no effect on the physiology of the intestine.

Deletion of GABRA1 in $LGR5^+$ ISCs or the administration of bicuculline prevented mouse small intestinal organoids against 5-FU– or irradiation-induced apoptosis

$LGR5^+$ ISCs play vital roles in chemoradiotherapy-induced enterotoxicity and intestinal regeneration (Barker et al., 2012; Yu, 2013). To explore whether GABRA1 in $LGR5^+$ ISCs has any effect on chemoradiotherapy-induced intestinal injury, we generated mice ($Gabra1^{Lgr5\text{-}KO}$) by crossing $Lgr5^{EGFP\text{-}IRES\text{-}CreERT2}$ mice with homozygous floxed alleles of *Gabra1* mice ($Gabra1^{flox/flox}$), and an ex vivo intestinal organoid culture system was used to explore its potential for chemoradioprotection (Clevers, 2016). We noticed that 5-FU (2.5 μM)– or irradiation (1 Gy)-induced organoid loss and growth suppression were less severe in the $Gabra1^{Lgr5\text{-}KO}$ group than in the control group (Fig. 2, A and C). The disappearance of ISCs is generally accepted to be the cause of intestinal injury after chemoradiotherapy (Berger et al., 2006). We found that $LGR5^+$ ISCs in $Gabra1^{Lgr5\text{-}KO}$ mice were well preserved 2 d after 5-FU or irradiation treatment (Fig. 2, E and F). Moreover, the expressions of phospho-P53 (p-P53), γ-H2AX, and Cleaved Caspase 3 were decreased in the $Gabra1^{Lgr5\text{-}KO}$ organoids compared with the control ($Lgr5^{EGFP}$) organoids 36 h after 5-FU treatment (Fig. 2 B) or 18 h after irradiation treatment (Fig. 2 D). In general, our data suggest that GABRA1 in $LGR5^+$ ISCs plays a vital role in chemoradiotherapy-induced IEC apoptosis.

Bicuculline is a well-known antagonist of $GABA_AR$. Therefore, we examined whether bicuculline had any effect on 5-FU- or irradiation-induced intestinal toxicity. Small intestinal organoids were treated with bicuculline (1 μM) 1 h before 5-FU (2.5 μM) or irradiation (1 Gy) treatment. As expected, bicuculline rescued the organoids from 5-FU– or irradiation-induced toxicity and improved the growth of ISCs (Fig. 2, G and I). In addition, bicuculline-treated organoids demonstrated an obvious decrease in the protein levels of p-P53, γ-H2AX, and Cleaved Caspase 3 compared with vehicle organoids 36 h after 5-FU treatment (Fig. 2 H) or 18 h after irradiation treatment (Fig. 2 J), which further suggested that inhibition of $GABA_AR$ could reduce P53-dependent crypt cell apoptosis, thereby alleviating 5-FU– or irradiation-induced toxicity.

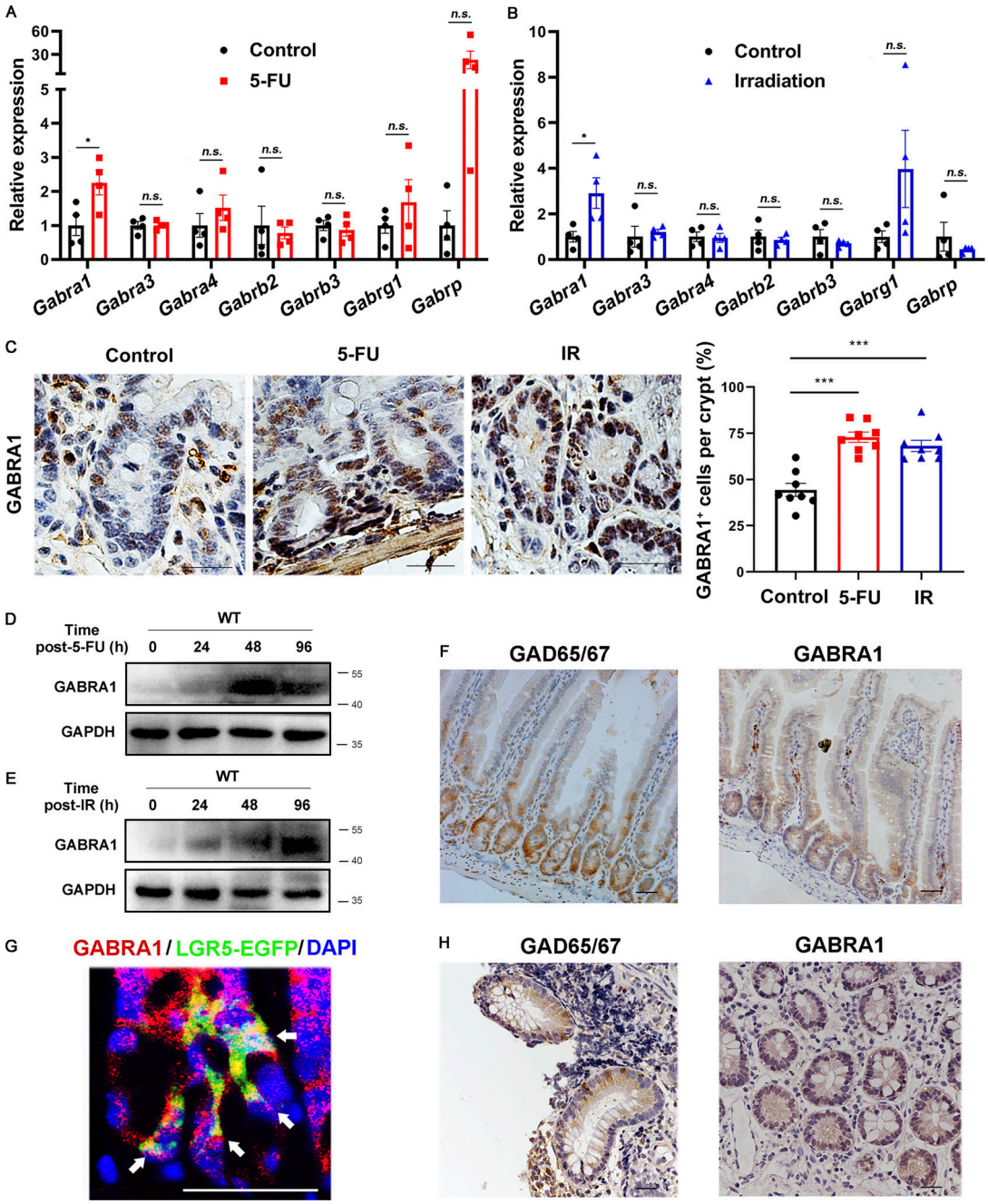

Figure 1. **GABA$_A$R α1 was upregulated in mouse small intestinal crypts after 5-FU or irradiation treatment. (A and B)** RT-PCR analysis of several GABA$_A$R subunits from mouse intestinal tissues with or without 5-FU (A) or irradiation treatment (B). **(C)** Immunohistochemistry staining for the expression of GABRA1 in mouse small intestinal crypts after 5-FU or irradiation treatment. Scale bar, 50 µm. Histogram demonstrating the percentages of GABRA1$^+$ cells in each crypt. **(D and E)** Immunoblot of GABRA1 in mouse small intestinal crypts at indicated time points after 5-FU (D) or irradiation treatment (E). **(F)** Immunohistochemistry staining for the expression of GAD65/67 and GABRA1 in mouse small intestine. Scale bar, 50 µm. **(G)** GABRA1 (red) and GFP (LGR5, green) immunofluorescence staining in mouse small intestinal crypts. Scale bar, 50 µm. Arrows indicate GABRA1$^+$/LGR5-EGFP$^+$ cell pairs, DAPI (blue) was used to stain nuclei. **(H)** Immunohistochemistry staining for the expression of GAD65/67 and GABRA1 in the small intestine of humans. Scale bar, 50 µm. In A–C, values are means ± SEM; *n* = 4 mice per group. n.s., not significant; *, P < 0.05; and ***, P < 0.001 (two-tailed Student's *t* test). Data are representative of two (A, B, D, and E) or three (C, F, G, and H) independent experiments. Source data are available for this figure: SourceData F1.

Deletion of GABRA1 in IECs protected against 5-FU– or irradiation-induced apoptosis of IECs in mice

Next, we explored the role of GABRA1 in IECs in 5-FU– or irradiation-induced intestinal toxicity in vivo. *Gabra1$^{flox/flox}$* and *Gabra1$^{IEC\text{-}KO}$* mice were treated with 5-FU (30 mg/kg i.p.; Fig. 3 A) or irradiation (6 Gy, total body irradiation [TBI], once; Fig. 3 I), and the jejunum was obtained 5 d after 5-FU treatment or 4 d after irradiation treatment for further analysis. Treatment with 5-FU or irradiation impaired the villi in the *Gabra1$^{flox/flox}$* group, and interestingly, this damage response was alleviated in the

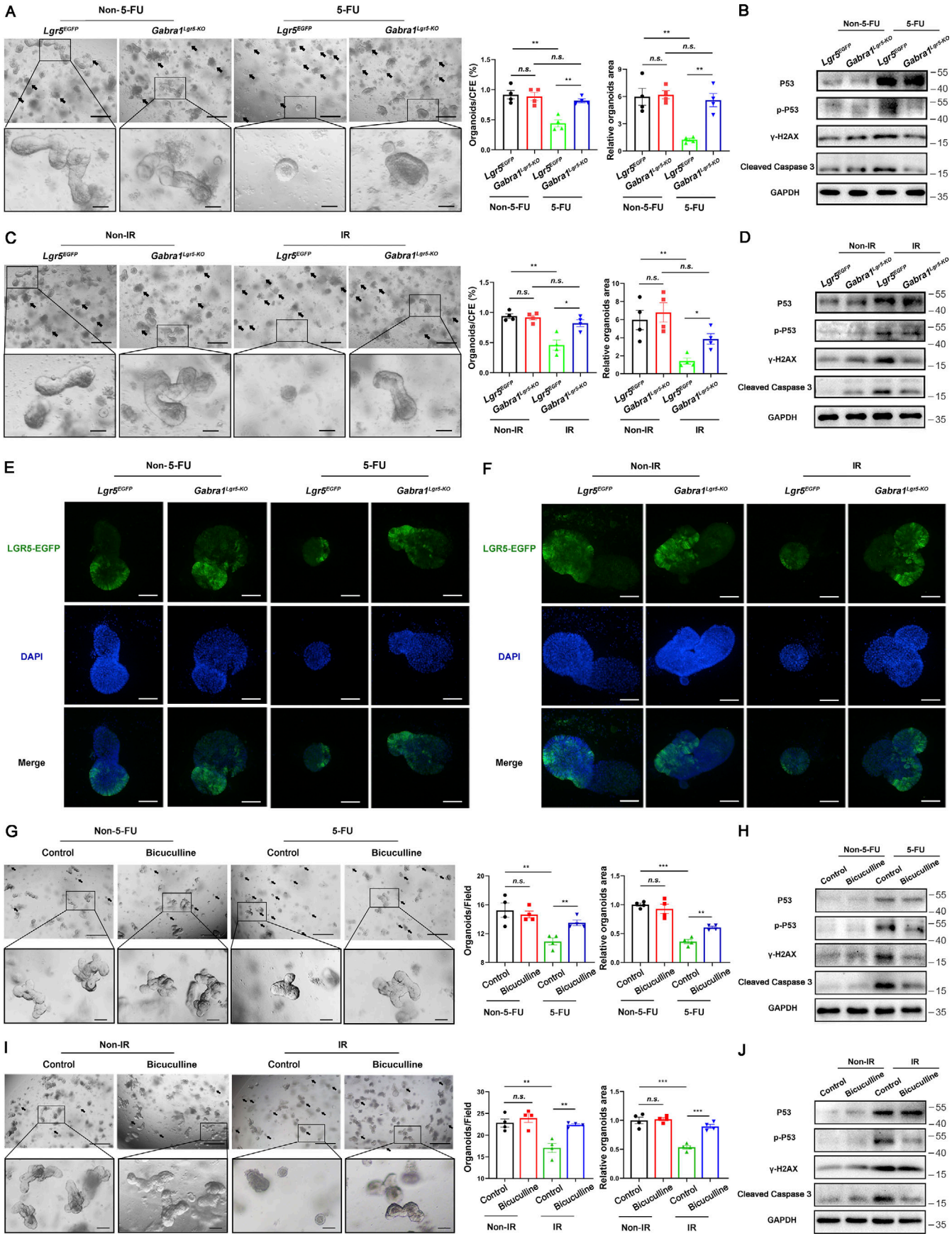

Figure 2. **Deletion of GABRA1 in LGR5⁺ ISCs or administration of bicuculline prevented mouse small intestinal organoids against 5-FU– or irradiation-induced apoptosis. (A and C)** Representative images of *Lgr5*$^{EGFP\text{-}IRES\text{-}CreERT2}$ (*Lgr5*^{EGFP}) and *Gabra1*$^{Lgr5\text{-}KO}$ mice intestinal organoids 2 d after 5-FU (2.5 µM; A) or irradiation (1 Gy) treatment (C). Scale bar, 500 µm (upper) or 100 µm (bottom). Arrows indicate dead organoids. Histograms of organoids quantitation and area per field relative to the measurement on day 1. **(B and D)** Western blots for P53, p-P53, γ-H2AX, and Cleaved Caspase 3 from organoids 36 h after 5-FU treatment (B) or 18 h after irradiation treatment (D). **(E and F)** GFP (LGR5, green) immunofluorescence in intestinal organoids 2 d after 5-FU (E) or irradiation treatment (F). Scale bar, 25 µm. **(G and I)** Representative images of C57BL/6 mouse intestinal organoids 2 d after 5-FU (G) or irradiation treatment (I). Organoids were treated with vehicle or bicuculline (1 µM). Scale bar, 500 µm (upper) or 100 µm (bottom). **(H and J)** Western blots for P53, p-P53, γ-H2AX, and Cleaved Caspase 3 from organoids 36 h after 5-FU treatment (H) or 18 h after irradiation treatment (J). In A, C, G, and I, values are means ± SEM. n.s., not significant; *, P < 0.05; **, P < 0.01; and ***, P < 0.001 (two-tailed Student's *t* test). Data are representative of at least three (A–J) independent experiments. Source data are available for this figure: SourceData F2.

Gabra1$^{IEC\text{-}KO}$ group (1.2-fold and 1.1-fold; Fig. 3, B and J). Compared with the *Gabra1*$^{flox/flox}$ group, the *Gabra1*$^{IEC\text{-}KO}$ group had many more TACs (1.2-fold and 1.9-fold; Fig. 3, C and K) and BrdU⁺ cells (1.5-fold and 1.4-fold; Fig. 3, D and L) 5 d after 5-FU treatment or 4 d after irradiation treatment. Owing to the limitations of LGR5 antibody application in immunohistochemistry, we used another ISC marker, OLFM4, to detect ISCs in mice without the *Lgr5-EGFP* marking allele (Gregorieff et al., 2015). The results showed that the number of OLFM4⁺ ISCs in *Gabra1*$^{flox/flox}$ mice was much lower (2.2-fold and 1.4-fold) than that in the *Gabra1*$^{IEC\text{-}KO}$ group (Fig. 3, E and M). Then, we monitored crypt DNA damage by staining γ-H2AX foci and found that the number of γ-H2AX⁺ cells was lower (0.71-fold and 0.77-fold) in the *Gabra1*$^{IEC\text{-}KO}$ group than in the *Gabra1*$^{flox/flox}$ group (Fig. 3, F and N). GABRA1 deletion in IECs strongly reduced the levels of p-P53, γ-H2AX, and Cleaved Caspase 3 after 5 d of 5-FU treatment or 4 d of irradiation treatment (Fig. 3, G and O). Additionally, GABRA1 deletion in IECs decreased 5-FU (200 mg/kg, i.p.)– or irradiation (10 Gy, TBI)-induced lethality (Fig. 3, H and P). These data demonstrate that the absence of *Gabra1* in IECs profoundly alters intestinal proliferation and apoptosis in response to chemoradiotherapy-induced DNA damage in vivo.

LGR5⁺ ISCs were the critical target of $GABA_AR$ signaling in reducing IEC apoptosis triggered by chemoradiotherapy

Considering that the depletion of GABRA1 in LGR5⁺ ISCs alleviated the damage generated by 5-FU or irradiation in mouse intestinal organoids, we hypothesized that the protective effect of depleting GABRA1 in IECs may be due to the loss of GABRA1 in ISCs. Therefore, we treated *Gabra1*$^{Lgr5\text{-}KO}$ mice and their littermate control mice (*Lgr5*$^{EGFP\text{-}IRES\text{-}CreERT2}$) with 5-FU (30 mg/kg, i.p.; Fig. 4 A) or irradiation (6 Gy, TBI, once; Fig. 4 I) 5 d after tamoxifen administration (2 mg per mouse, i.p.). The jejunum was obtained 5 d after 5-FU treatment or 4 d after irradiation treatment for further analysis. Our results showed that the *Gabra1*$^{Lgr5\text{-}KO}$ group displayed a better-preserved intestinal structure than the control group (1.4-fold and 1.4-fold; Fig. 4, B and J). Furthermore, 5-FU or irradiation induced an obvious loss of TACs in the control group, whereas it was significantly suppressed in the *Gabra1*$^{Lgr5\text{-}KO}$ group (1.5-fold and 1.7-fold; Fig. 4, C and K), along with enhanced proliferation capacity (1.7-fold and 2.1-fold; Fig. 4, D and L) 5 d after 5-FU treatment or 4 d after irradiation treatment. In addition, we observed strong protection against the loss of OLFM4⁺ (1.3-fold and 1.7-fold; Fig. 4, E and M) and LGR5⁺ (2.4-fold and 2.6-fold; Fig. 4, F and N) ISCs by GABRA1 deletion. Moreover, we found that the levels of p-P53, γ-H2AX, and Cleaved Caspase 3 were significantly decreased in IECs in the *Gabra1*$^{Lgr5\text{-}KO}$ group 5 d after 5-FU treatment (Fig. 4 G) or 4 d after irradiation treatment (Fig. 4 O), indicating that there was less P53-dependent apoptosis in *Gabra1*$^{Lgr5\text{-}KO}$ group. Surprisingly, there was a 40% survival rate of *Gabra1*$^{Lgr5\text{-}KO}$ mice receiving a lethal dose of 5-FU, whereas this same dose caused the death of all control mice within 11 d (Fig. 4 H). After 10 Gy of TBI exposure, the survival rate of *Gabra1*$^{Lgr5\text{-}KO}$ mice was much higher than that of the control mice (Fig. 4 P).

Next, we explored whether depletion of GABRA1 in LGR5⁺ ISCs could reduce high-dose irradiation-induced apoptosis in ISCs; *Gabra1*$^{Lgr5\text{-}KO}$ mice and their littermate control mice (*Lgr5*$^{EGFP\text{-}IRES\text{-}CreERT2}$, *Lgr5*^{EGFP}) were exposed to 15 Gy whole abdominal irradiation (WAI; Fig. 5 A). At 4 h after irradiation, immunofluorescence results showed that GABRA1 deletion in LGR5⁺ ISCs reduced cleaved Caspase 3⁺ LGR5⁺ ISCs by almost 40%, as observed in *Lgr5*^{EGFP} mice (Fig. 5 B). At 24 h after irradiation, we found that LGR5⁺ ISCs were reduced by >60% in *Lgr5*^{EGFP} mice, whereas more LGR5⁺ ISCs were observed in the *Gabra1*$^{Lgr5\text{-}KO}$ group (Fig. 5 C), and the levels of apoptotic P53 targets were also lower in *Gabra1*$^{Lgr5\text{-}KO}$ group (Fig. 5 E). Notably, the average villus length and crypt depth of the small intestine in *Gabra1*$^{Lgr5\text{-}KO}$mice were 1.3-fold and 1.4-fold higher than those in their littermate control mice (Fig. 5 D), along with more LGR5⁺ ISCs (1.8-fold; Fig. 5 C) 48 h after 15 Gy WAI. Moreover, the number of LGR5⁺ ISCs (Fig. 5 C) and crypt depth (Fig. 5 D) in *Gabra1*$^{Lgr5\text{-}KO}$ group recovered more rapidly than those in their littermate control mice 96 h after 15 Gy WAI. Additionally, *Gabra1*$^{Lgr5\text{-}KO}$ mice had a higher survival rate than control mice after 15 Gy WAI exposures (Fig. 5 F).

These data imply that GABRA1 in LGR5⁺ ISCs played an essential role in chemoradiotherapy-induced IEC apoptosis in vivo.

Bicuculline treatment protected against 5-FU- or irradiation-induced intestinal DNA damage and lethality in mice

To examine the efficacy of the $GABA_AR$ antagonist bicuculline in vivo, we treated WT mice with bicuculline (2 mg/kg, i.p.) or a vehicle along with 5-FU (30 mg/kg, i.p.; Fig. S2 A) or irradiation treatment (6 Gy, TBI, once; Fig. S2 H). Treatment with bicuculline greatly alleviated 5-FU– or irradiation-induced shortening of the villus length (1.3-fold and 1.7-fold; Fig. S2, B and I). Besides, 5 d after 5-FU treatment or 4 d after irradiation treatment, the number of TACs (1.4-fold and 1.2-fold; Fig. S2, C and J) and their proliferative capacity (1.6-fold and 1.4-fold; Fig. S2, D

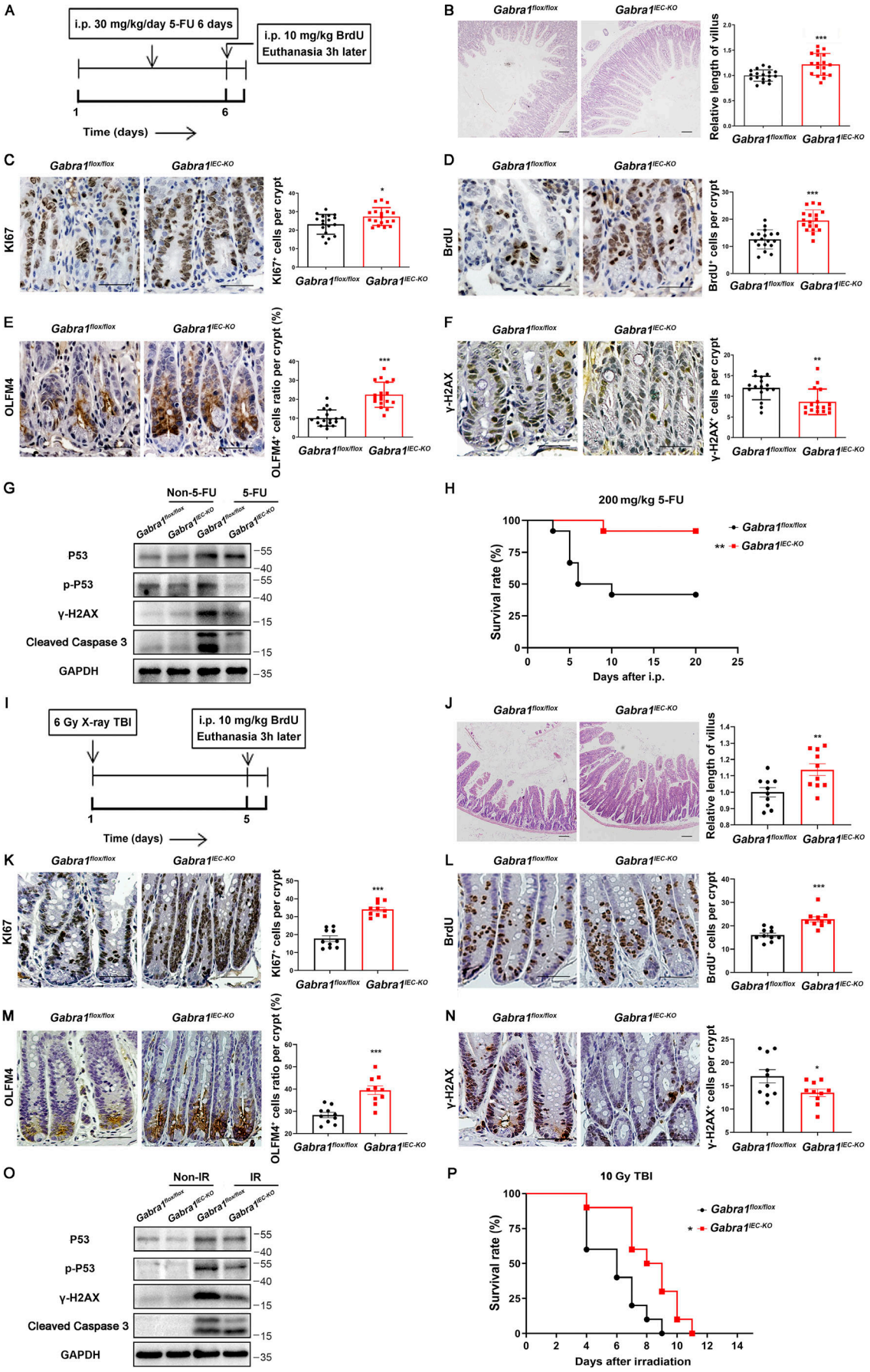

Figure 3. **GABRA1 deletion in IECs reduced 5-FU– or irradiation-induced apoptosis of IECs in mice.** *Gabra1*$^{IEC\text{-}KO}$ mice and their littermate control mice (*Gabra1*$^{flox/flox}$) were treated with 5-FU (30 mg/kg, i.p., for 6 d) or irradiation (6 Gy, TBI, once). For survival analysis, mice with indicated genotypes were treated with 5-FU (200 mg/kg, i.p.) or irradiation (10 Gy, TBI) once. **(A)** Schematic diagram of 5-FU treatment to indicated mice. **(B)** Representative images of H&E staining of the jejunum tissues from mice treated as in A. Scale bar, 100 µm. The relative length of villus is relative to control. **(C–F)** Representative images of KI67 (C), BrdU (D), OLFM4 (E), and γ-H2AX (F) staining in the jejunum tissues from mice treated as in A. Scale bar, 50 µm. Histogram demonstrating the number of staining-positive cells per crypt. **(G)** Immunoblots of P53, p-P53, γ-H2AX, and Cleaved Caspase 3 in the intestinal mucosa from mice treated as in A. **(H)** Log-rank (Mantel-Cox) survival analysis of indicated mice treated with 5-FU on day 0. *Gabra1*$^{flox/flox}$ versus *Gabra1*$^{IEC\text{-}KO}$, n = 12 mice per group; **, P < 0.01 (log-rank [Mantel-Cox] test). In B–F, values are means ± SEM; n = 9 mice per group. *, P < 0.05; **, P < 0.01; and ***, P < 0.001 (two-tailed Student's t test). **(I)** Schematic diagram of irradiation treatment to indicated mice. **(J)** Representative images of H&E staining of the jejunum tissues from mice treated as in I. Scale bar, 100 µm. **(K–N)** Representative images of KI67 (K), BrdU (L), OLFM4 (M), and γ-H2AX (N) staining of the jejunum tissues from mice treated as in I. Scale bar, 50 µm. **(O)** Immunoblots of P53, p-P53, γ-H2AX, and Cleaved Caspase 3 in the intestinal mucosa from mice treated as in I. **(P)** Log-rank (Mantel-Cox) survival analysis of indicated mice treated with irradiation on day 0. *Gabra1*$^{flox/flox}$ versus *Gabra1*$^{IEC\text{-}KO}$, n = 10 mice per group; *, P < 0.05 (log-rank [Mantel-Cox] test). In J–N, values are means ± SEM; n = 5 mice per group. *, P < 0.05; and ***, P < 0.001 (two-tailed Student's t test). Data are representative of two (H and P) or three (B–G, and J–O) independent experiments. Source data are available for this figure: SourceData F3.

and K) were significantly higher after bicuculline treatment. Moreover, we noticed that bicuculline prevented the loss of OLFM4$^+$ ISCs (1.8-fold and 1.9-fold; Fig. S2, E and L) after chemoradiotherapy. We also monitored crypt DNA damage by analyzing γ-H2AX, p-P53, and Cleaved Caspase 3 expressions, which were lower in the bicuculline treatment group than in the control group (Fig. S2, F, G, M and N). Taken together, these results further demonstrated that inhibition of $GABA_AR$ could protect the intestine by reducing DNA double-strand breaks and downstream P53-dependent apoptotic pathways caused by 5-FU or irradiation treatment.

Bicuculline inhibited L-type Ca^{2+} channel and oxidative stress to suppress 5-FU– or irradiation-induced DNA damage via activation of the PIKK pathway

To investigate which downstream effector of $GABA_AR$ signaling is involved in the occurrence of P53-dependent apoptosis induced by 5-FU or irradiation treatment, organoids were treated with irradiation (1 Gy) 1 h after vehicle or bicuculline (1 µM) treatment, and total ATM, phospho-ATM (p-ATM, Ser1981), and γ-H2AX were detected 1 h after irradiation treatment. In the absence of irradiation treatment, bicuculline had no effect on these proteins (Fig. S3 A). Interestingly, the levels of ATM, p-ATM, and γ-H2AX decreased in the bicuculline-treated group after irradiation compared to the control group (Fig. 6 A), whereas $GABA_AR$ agonist muscimol (1 µM) increased their levels (Fig. S3 C and Fig. 6 C). Similarly, muscimol did not affect the survival or growth of organoids within 2 d without irradiation treatment (Fig. S3 B). Interestingly, muscimol aggravated irradiation-induced organoid toxicity, which was reversed by a specific p-ATM inhibitor, KU-60019 (1 µM; Fig. 6, B and C). These data suggest that bicuculline reduced the P53 downstream apoptosis pathway and promoted organoid survival and growth upon irradiation by inhibiting ATM.

ATM, a primary responder to double-strands breaks, is activated by DNA damage (Bakkenist and Kastan, 2003). Therefore, we sought to detect the amount of DNA damage by using the comet assay (Olive and Banath, 2006). We found that bicuculline or muscimol treatment had no impact on the DNA damage level of organoids in the absence of 5-FU or irradiation treatment (Fig. S3, D and E). After exposure to 5-FU (2.5 µM) or irradiation (1 Gy) treatment, organoids treated with bicuculline had less DNA damage than the vehicle group, including less tail DNA%, shorter tail length, and lower tail moment, whereas muscimol-treated organoids showed more severe injury (Fig. 6, D and E), which implied that $GABA_AR$ regulated organoid survival by affecting DNA damage.

5-FU (Dey et al., 2020) or irradiation (Lee et al., 2017) treatment caused DNA damage either directly or indirectly via ROS generation. Thus, we measured the ROS levels in organoids with corresponding treatments using 8-OHdG staining, a biomarker of oxidative stress. We found that bicuculline or muscimol treatment did not alter organoid ROS levels without 5-FU or irradiation treatment (Fig. S3, F and G); however, bicuculline treatment suppressed 5-FU- or irradiation-induced ROS generation, muscimol treatment showed an enhanced ROS generation (Fig. 6, F and G). Collectively, these data demonstrate that bicuculline functions as an antioxidant.

5-FU or irradiation treatment leads to the accumulation of intracellular calcium in colon carcinoma (Can et al., 2013) and human embryonic kidney cells (Guleria et al., 2018). Here, we found that voltage-dependent L-type calcium channel subunit alpha-1C (CACNA1C) was expressed on LGR5$^+$ ISCs (Fig. 7 A). Calcium imaging showed that 5-FU or irradiation induced intracellular calcium accumulation in mouse small intestinal crypt cells (Fig. 7 B).

There is a close connection between L-type Ca^{2+} channel activation and ROS production (Johnstone and Hool, 2014). Therefore, we sought to determine whether bicuculline or muscimol alters ROS levels by mediating L-type Ca^{2+} channels. The data showed that 5-FU– or irradiation-induced organoid apoptosis was suppressed by nifedipine (0.1 µM) treatment alone, a dihydropyridine calcium channel blocking agent, which was similar to the chemoradioprotection effect of bicuculline on organoids (Fig. 7, C and D). Besides, nifedipine alleviated the muscimol-induced aggravation of 5-FU– or irradiation-induced organoid toxicity (Fig. 7, C and D). These results indicate that bicuculline inhibited L-type Ca^{2+} channels, thereby reducing cellular ROS levels induced by 5-FU or irradiation treatment.

Bicuculline did not affect antitumor activity of 5-FU or irradiation treatment

To determine whether bicuculline affects cancer cell sensitivity to chemoradiotherapy, we first used *Apc*$^{Min/+}$ mice as a

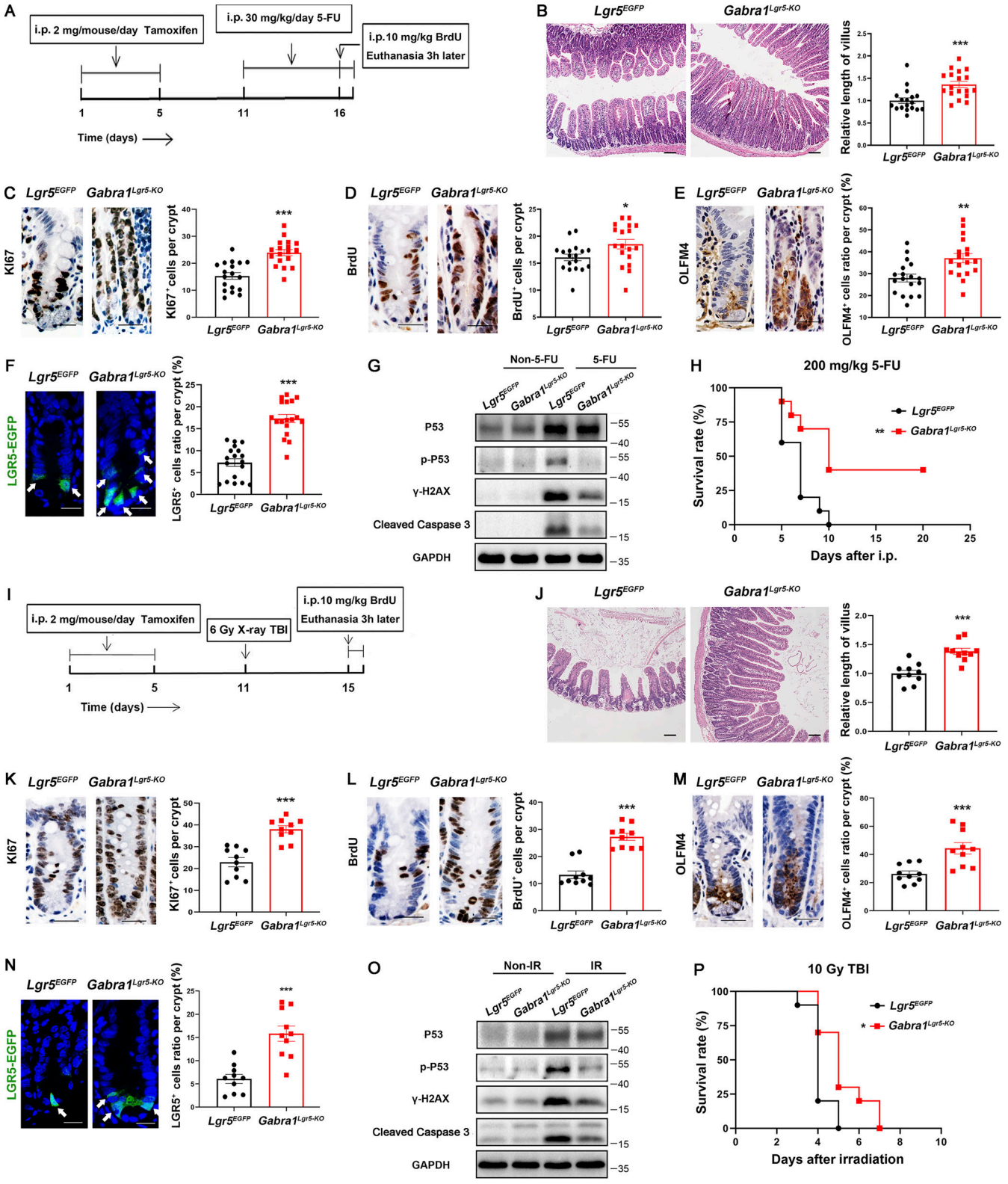

Figure 4. **Loss of *Gabra1* in LGR5⁺ stem cells protected mice against 5-FU– or irradiation-induced intestinal injury.** *Gabra1*$^{Lgr5\text{-}KO}$ mice and their littermate control mice (*Lgr5*$^{EGFP\text{-}IRES\text{-}CreERT2}$, *Lgr5*^{EGFP}) received tamoxifen (2 mg per mouse, i.p.) over a 5-d period. Then, 5-FU (30 mg/kg, i.p., 6 d) or irradiation (6 Gy, TBI, once) was given. For survival analysis, mice with indicated genotypes were treated with 5-FU (200 mg/kg, i.p.) or irradiation (10 Gy, TBI) once. **(A)** Schematic diagram of 5-FU treatment to indicated mice. **(B)** Representative images of H&E staining of the jejunum tissues from mice treated as in A. Scale bar, 100 µm. **(C–F)** Representative images of KI67 (C), BrdU (D), OLFM4 (E), and GFP (LGR5, green; F) staining of the jejunum tissues from mice treated as in A. Scale bar, 50 µm. Arrows indicate LGR5⁺ cells. **(G)** Immunoblots of P53, p-P53, γ-H2AX, and Cleaved Caspase 3 in the intestinal mucosa from mice treated as in A. **(H)** Log-rank (Mantel-Cox) survival analysis of indicated mice treated with 5-FU on day 0. *Lgr5*^{EGFP}versus *Gabra1*$^{Lgr5\text{-}KO}$, *n* = 10 mice per group; **, P < 0.01

(log-rank [Mantel-Cox] test). In B–F, values are means ± SEM; n = 9 mice per group. *, P < 0.05; **, P < 0.01; and ***, P < 0.001 (two-tailed Student's t test). **(I)** Schematic diagram of irradiation treatment to indicated mice. **(J)** Representative images of H&E staining of the jejunum tissues from mice treated as in I. Scale bar, 100 µm. **(K–N)** Representative images of KI67 (K), BrdU (L), OLFM4 (M), and GFP (LGR5, green; N) staining of the jejunum tissues from mice treated as in I. Scale bar, 50 µm. Arrows indicate LGR5$^+$ cells. **(O)** Immunoblots of P53, p-P53, γ-H2AX, and Cleaved Caspase 3 in the intestinal mucosa from mice treated as in I. **(P)** Log-rank (Mantel-Cox) survival analysis of indicated mice treated with irradiation on day 0. *Lgr5*^{EGFP} versus *Gabra1*$^{Lgr5\text{-}KO}$, n = 10 mice per group; *, P < 0.05 (log-rank [Mantel-Cox] test). In J–N, values are means ± SEM; n = 5 mice per group. ***, P < 0.001 (two-tailed Student's t test). Data are representative of two (H and P) or three (B–G and J–O) independent experiments. Source data are available for this figure: SourceData F4.

spontaneous intestinal adenoma model (Fig. 8 A; Zhou et al., 2013). There were no significant changes in the tumor number (Fig. 8 B) and villus length (Fig. 8 C) between *Apc*$^{Min/+}$ mice treated with or without bicuculline (2 mg/kg, i.p.) in the absence of chemoradiotherapy. Notably, under the condition of 5-FU chemotherapy (30 mg/kg, i.p., 6 d) or abdominal radiotherapy (15 Gy, WAI, once), bicuculline treatment alleviated 5-FU– or irradiation-induced intestinal structure damage (Fig. 8 C) without affecting the tumor response to chemoradiotherapy (Fig. 8 B).

Moreover, we established subcutaneous Lewis lung carcinoma (LLC) tumors in immunocompetent WT mice. When tumors reached an average of 100 mm^3, mice were treated with bicuculline (2 mg/kg, i.p., once every 2 d) and 5-FU (100 mg/kg, i.p., once every 4 d) or irradiation (3 Gy, TBI, once every 4 d; Fig. 8, D and I). Indeed, treatment with bicuculline alone was indistinguishable from the control in terms of tumor growth (Fig. 8, E, G, J and L) or proliferating cell nuclear antigen (PCNA) levels (Fig. 8, F and K). Importantly, under chemoradiotherapy, bicuculline treatment (5-FU+Bicuculline or IR+Bicuculline) showed a tumor response similar to that of the control (5-FU or IR; Fig. 8, E and J), but the intestine from the bicuculline treatment group was highly resistant to chemoradiotherapy-induced intestinal structural damage (Fig. 8, H and M).

Fractionated abdominal radiotherapy is a commonly used radiotherapy regimen in the clinical setting (Erlandsson et al., 2017). Thus, a MC38 (murine colon adenocarcinoma) tumor-bearing mouse model was used to further evaluate the effects of bicuculline on normal and malignant tissues after fractionated abdominal radiotherapy (4 Gy, WAI/fraction; Fig. S4 A). There was no significant difference in tumor growth (Fig. S4, B and D) or PCNA levels (Fig. S4 C) between the control and bicuculline-treated groups with or without fractionated abdominal radiotherapy. Nevertheless, compared with the control group (IR), bicuculline-treated mice (IR+Bicuculline) exhibited obvious resistance to fractionated abdominal radiotherapy-induced intestinal damage, including less villus shortening (1.3-fold; Fig. S4 E), higher number of TACs (1.5-fold; Fig. S4 F) along with enhanced proliferation capacity (1.4-fold; Fig. S4 G), and less OLFM4$^+$ ISC loss (2.0-fold; Fig. S4 H). These results demonstrate that bicuculline attenuated 5-FU– or irradiation-induced enterotoxicity but did not accelerate tumor development or desensitization to chemoradiotherapy in these murine models.

Flumazenil protected against 5-FU– or irradiation-induced IEC apoptosis

Flumazenil, a 1,4-imidazobenzodiazepine, has been generally used to antagonize the hypnotic and sedative effects of benzodiazepines on GABA$_A$R in the clinical setting (Brogden and Goa, 1991). To examine the efficacy of flumazenil in 5-FU– or irradiation-induced enterotoxicity, we evaluated small intestine injury induced by 5-FU (30 mg/kg, i.p.; Fig. 9 A) or irradiation (6 Gy, TBI, once; Fig. 9 H) with or without flumazenil treatment (1 mg/kg, i.p.). We found that the jejunum crypt–villus architecture in mice treated with flumazenil was well preserved (1.4-fold and 1.2-fold; Fig. 9, B and I) 5 d after 5-FU treatment or 4 d after irradiation treatment. The TACs number (1.3-fold and 1.2-fold; Fig. 9, C and J), their proliferation ability (1.3-fold and 1.2-fold; Fig. 9, D and K), and OLFM4$^+$ ISC number (1.4-fold and 1.5-fold; Fig. 9, E and L) significantly increased in flumazenil-treated mice compared with the vehicle-treated group. We also found that flumazenil treatment greatly diminished 5-FU– (0.64-fold; Fig. 9 F) or irradiation (0.76-fold; Fig. 9 M)-induced DNA double-strand break. Notably, flumazenil treatment increased the survival rate of mice after treatment with lethal doses of 5-FU (Fig. 9 G) or irradiation (Fig. 9 N). To further analyze the effect of flumazenil on human ISC activity, we used a human colonic organoid culture system exposed to 5-FU or irradiation (Fujii et al., 2015). Human organoids were treated with 5-FU (2.5 µM) or irradiation (1 Gy) 1 h after flumazenil (1 µM) or vehicle treatment. The results showed that the number and size of human organoids increased in the flumazenil-treated group than in the vehicle treatment group 48 h after 5-FU or irradiation treatment, (Fig. 9, O and P). Taken together, these data suggest that flumazenil alleviates 5-FU- or irradiation-induced intestinal injury.

Discussion

Gastrointestinal syndrome caused by chemoradiotherapy limits the maximum chemotherapy dose to the lower abdomen, and may also decrease patients' quality of life (Andreyev, 2016). The identification of new targets to develop adjuvants will be beneficial for cancer care and oncological treatments. In this study, we uncovered a novel role for GABA$_A$R inhibitors in reducing chemoradiotherapy-induced intestinal injury by preventing ROS-induced ISC apoptosis. The entire GABAergic system was expressed in the intestinal epithelium and lamina propria without affecting the homeostasis of ISCs. However, loss of *Gabra1* alleviated chemoradiotherapy-induced intestinal injury in both the intestinal epithelium and stem cells. Intriguingly, GABA$_A$R inhibitors did not interfere with the antitumor activities of chemoradiotherapy, suggesting that the FDA-approved flumazenil is a promising drug for clinical combination with chemoradiotherapy.

GABA plays a role beyond synapses and is involved in regulating the proliferation of embryonic stem cells, neural crest stem cells (Andang et al., 2008), and hematopoietic stem and

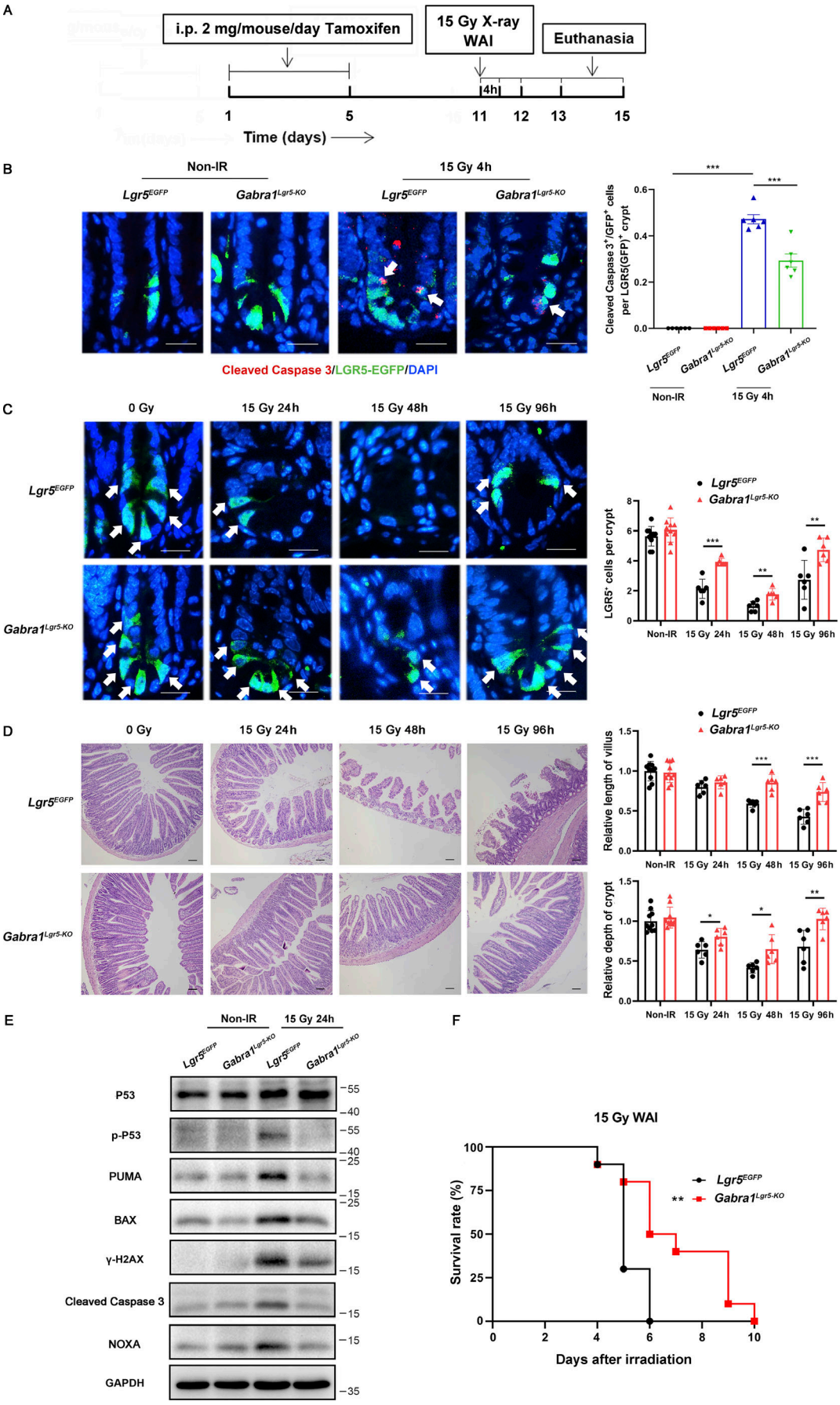

Figure 5. **Deletion of GABRA1 in LGR5⁺ ISCs attenuated intestinal damage in response to WAI. (A)** Schematic diagram of irradiation treatment (15 Gy, WAI, once) to *Gabra1*$^{Lgr5\text{-}KO}$ mice and their littermate control mice (*Lgr5*$^{EGFP\text{-}IRES\text{-}CreERT2}$, *Lgr5*^{EGFP}). **(B)** Cleaved Caspase 3 (red) and GFP (LGR5, green) immunofluorescence staining of the intestinal crypts of indicated mice 4 h after irradiation treatment. Scale bar, 25 µm. Asterisks indicate Cleaved Caspase 3⁺/LGR5⁺ cell pairs. **(C)** Representative images of GFP (LGR5, green) immunofluorescence staining of the jejunum tissues from mice treated as in A. Scale bar, 25 µm. Arrows indicate LGR5⁺ ISCs. **(D)** Representative images of H&E staining of the jejunum tissues from mice treated as in A. Scale bar, 100 µm. **(E)** Immunoblots of P53, p-P53, PUMA, BAX, γ-H2AX, Cleaved Caspase 3, and NOXA in the jejunum tissues of indicated mice 24 h after irradiation treatment. **(F)** Log-rank (Mantel-Cox) survival analysis of indicated mice treated with irradiation (15 Gy, WAI, once) on day 0. *Lgr5*^{EGFP} versus *Gabra1*$^{Lgr5\text{-}KO}$, *n* = 10 mice per group; **, P < 0.01 (log-rank [Mantel-Cox] test). In B–D, values are means ± SEM. *n* = indicated mice per group. *, P < 0.05; **, P < 0.01; and ***, P < 0.001 (two-tailed Student's *t* test). Data are representative of at least two (B–F) independent experiments. Source data are available for this figure: SourceData F5.

progenitor cells (Elujoba-Bridenstine et al., 2020; Zhu et al., 2019). Moreover, multiple studies have reported that GABAergic signaling cells autonomously modulate immune responses in immune cells (Bjurstöm et al., 2008; Jin et al., 2013; Kim et al., 2018; Zheng et al., 2021). Our findings provide evidence that $GABA_AR$ signaling does not change the physiology of ISCs and selectively protects against chemoradiotherapy-induced DNA damage response in LGR5⁺ ISCs. Although overexpression of $GABA_AR$ δ accelerated colorectal cancer cell progression (Niu et al., 2020) and activation of the $GABA_BR$ pathway inhibited colorectal cell proliferation by arresting the cell cycle (Shu et al., 2016), we did not observe that inhibition of the $GABA_AR$ pathway could affect colon cancer proliferation (Fig. S5 B), which implies that GABA might have different functions in colon cancer through different $GABA_AR$ subunits or $GABA_BR$ pathways.

Interestingly, inhibition of $GABA_AR$ selectively protected ISCs and the intestinal epithelium, but not tumor cells, in response to chemoradiotherapy. We found that the expression distribution of *Gabra1* mRNA in colon adenocarcinoma tissues was much lower (4.8-fold) than that in normal colorectal tissues (Fig. S5 C) by comparing and analyzing the RNA-seq data in The Cancer Genome Atlas (TCGA) and Genotype-Tissue Expression (GTEx) databases. Additionally, inhibition of $GABA_AR$ attenuated chemoradiotherapy-induced enterotoxicity by reducing P53-dependent apoptosis of the normal intestinal epithelium. However, P53 mutations are common in tumor cells (Olivier et al., 2010), which means that inhibiting $GABA_AR$ does not reduce the P53-dependent apoptosis of tumor cells induced by chemoradiotherapy. Although we found that the chemoradioprotective role of inhibiting $GABA_AR$ may result from reduced IEC apoptosis, we cannot exclude other possibilities. For example, radiation proctopathy is mediated by the activation of platelet-derived growth factor receptor (PDGFR; Lu et al., 2021), and there is an interaction between the activation status of $GABA_AR$ and PDGFR with the bridge of phospholipase C-γ (Valenzuela et al., 1995), which implies that the role of $GABA_AR$ in irradiated IECs might also depend on the PDGFR-C-X-C motif chemokine receptor 4 axis.

There are no FDA-approved drugs for treating radiation enteropathy (Hauer-Jensen et al., 2014). The $GABA_AR$ inhibitor flumazenil is cheap and has been used to treat benzodiazepine overdoses and safely reverse anesthesia for 30 yr. Our data support the protective role of $GABA_AR$ inhibition in chemoradiotherapy-induced injury of mouse organoids by reducing free radical formation. When ionizing radiation is absorbed by small molecules surrounding cellular biomacromolecules or chemicals that are transported into the mitochondrion, ROS form and react with cellular DNA to cause a DNA damage response (Smith et al., 2017). Many oncologists believe that antioxidants may weaken the free radical-killing function of chemoradiotherapy and should be avoided during treatment (D'Andrea, 2005). In contrast, there is no laboratory or clinical evidence supporting their claims (Moss, 2007), and our xenograft model study revealed that the protective ability of $GABA_AR$ inhibitors was restricted to the normal intestines. However, the mechanism of $GABA_AR$-selective protection in normal tissues needs to be explored in the future.

Effective treatment of cancers by chemoradiotherapy mainly relies on selectively killing cancer cells without affecting normal tissues (Gudkov and Komarova, 2010). Here, we demonstrated that inhibiting $GABA_AR$ is a promising strategy to specifically protect the intestine from chemoradiotherapy. Future studies are required to investigate the pharmacodynamics and tolerability of flumazenil in clinical settings with chemoradiotherapy.

Materials and methods

Mice

Gabra1$^{flox/flox}$ (JAX stock #004318), *Villin-Cre* (JAX stock #004586), *Lgr5*$^{EGFP\text{-}IRES\text{-}CreERT2}$ (JAX stock #008875), and *Apc*$^{Min/+}$ mice (JAX stock #002020) were purchased from Jackson Laboratory. WT (C57BL/6J) mice were purchased from Vital River Laboratory Animal Technology Co. All animal experiments were performed in accordance with the National Institutes of Health Guide for the Care and Use of Laboratory Animals with approval from the Scientific Investigation Board of Shandong University, Jinan, Shandong Province, China (#ECSBMSSDU2019-2-048).

Mice treatment

WT mice (C57BL/6J; 8–10 wk old), *Apc*$^{Min/+}$ mice (4 mo old), *Gabra1*$^{IEC\text{-}KO}$ (8–10 wk old), *Gabra1*$^{Lgr5\text{-}KO}$ (8–10 $^{wk\ old)}$ and littermate control mice (*Gabra1*$^{flox/flox}$ or *Lgr5*$^{EGFP\text{-}IRES\text{-}CreERT2}$, 8–10 wk old) were used in the chemoradiotherapy experiments, and the number of mice used in each group was indicated in the results of the corresponding experiments. Indicated mice were i.p. with 5-FU (30 mg/kg/d for 6 d as the therapeutic dose [Kim et al., 2005; Zhou et al., 2013]; 200 mg/kg once as the lethal high dose [Zhang et al., 2018]) or were irradiated (10 Gy TBI [Accarie et al., 2020] or 15 Gy WAI [Liu et al., 2016] per mouse once for survival analysis; 6 Gy TBI per mouse once [Dubois and Walker, 1988; Hendry and Otsuka, 2016] or 15 Gy WAI per mouse once [Liu

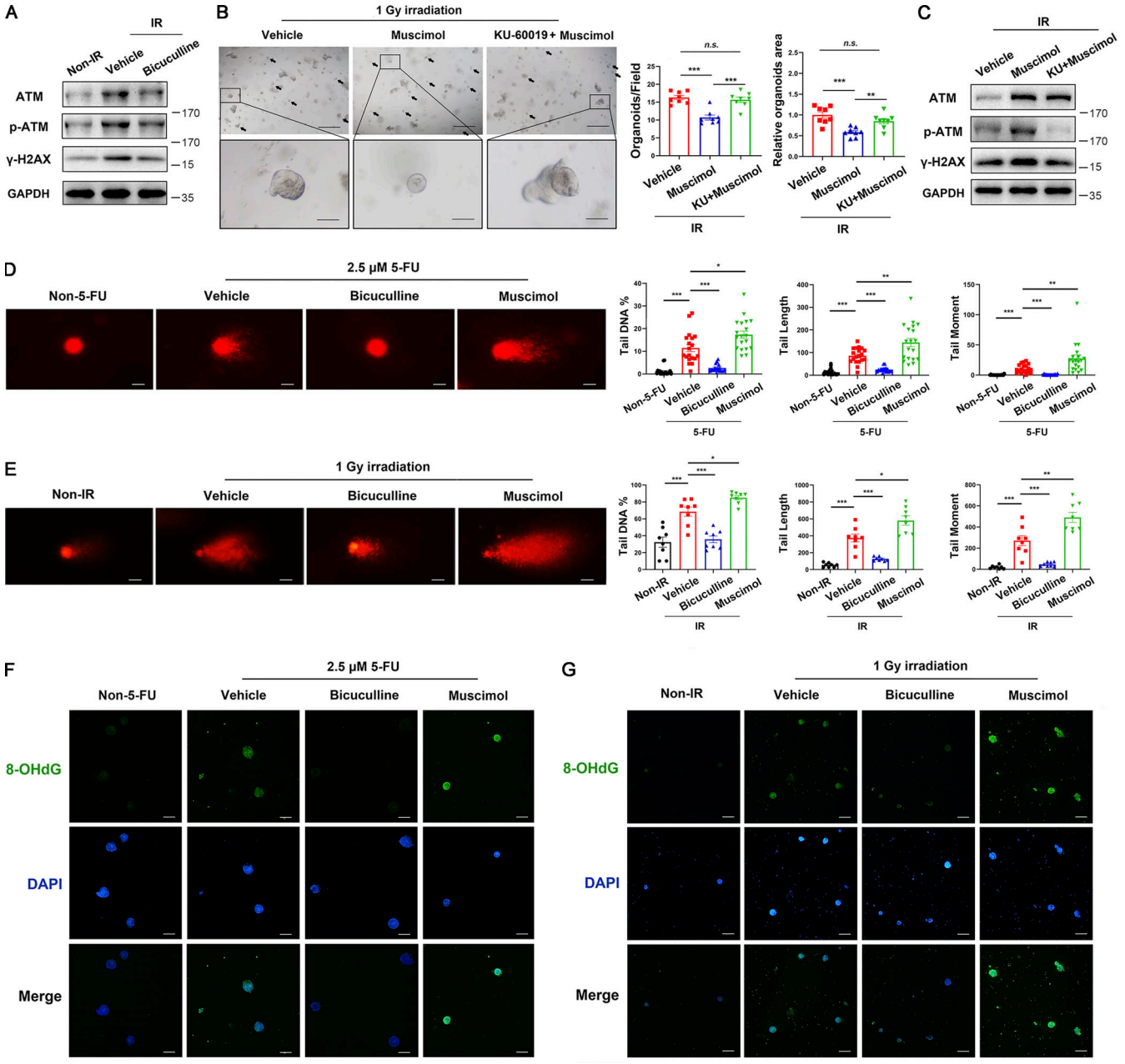

Figure 6. **Bicuculline treatment reduced 5-FU- or irradiation-induced ROS and DNA damage.** C57BL/6 mouse intestinal organoids were treated with vehicle, bicuculline (1 μM), muscimol (1 μM), or KU-60019 (1 μM) + muscimol (1 μM) 1 h before irradiation (1 Gy) treatment. **(A)** Immunoblots of ATM, p-ATM, and γ-H2AX in organoids 1 h after irradiation (1 Gy) treatment. **(B)** Representative images of organoids 2 d after irradiation treatment. Scale bar, 500 μm (upper) or 100 μm (bottom). Arrows indicate dead organoids. **(C)** Immunoblots of ATM, p-ATM, and γ-H2AX in organoids 30 min after irradiation treatment as in B. **(D and E)** Representative images of the comet assay of individual cells isolated from organoids 24 h after 5-FU (2.5 μM) treatment (D) or 1 h after irradiation (1 Gy) treatment (E). Scale bar, 25 μm. Histograms demonstrating the tail DNA %, tail length, and tail moment of each comet. **(F and G)** Representative immunofluorescence images of 8-OHdG (green) staining of organoids 24 h after 5-FU treatment (F) or 1 h after irradiation treatment (G). Scale bar, 100 μm. In B, D, and E, values are means ± SEM. *, $P < 0.05$; **, $P < 0.01$; and ***, $P < 0.001$ (two-tailed Student's *t* test). Data are representative of at least three (A–G) independent experiments. Source data are available for this figure: SourceData F6.

et al., 2016] for normal intestinal injury analysis). Bicuculline (2 mg/kg) was administered i.p. in both experiments. The jejunum was obtained 5 d after 5-FU treatment (30 mg/kg, i.p.) or 4 d after irradiation treatment (6 Gy, TBI, once) for further analysis in related mouse experiments. To measure cell proliferation, the mice were injected with BrdU (10 mg/kg, i.p.) 3 h before sacrifice. In addition, 4 million LLC cells or 2 million MC38 cells were injected into the flank of the WT mice. When the tumor volume was ~100 mm^3, the mice were treated with vehicle or bicuculline (2 mg/kg, i.p., once every 2 d) with or without 5-FU (100 mg/kg, i.p., once every 4 d) or irradiation (3 Gy, TBI or 4 Gy, WAI, once every 4 d) treatment. Fractionated abdominal irradiation (4 Gy WAI/fraction) was administered four times in total; once every 4 d (Chen et al., 2020). The mice

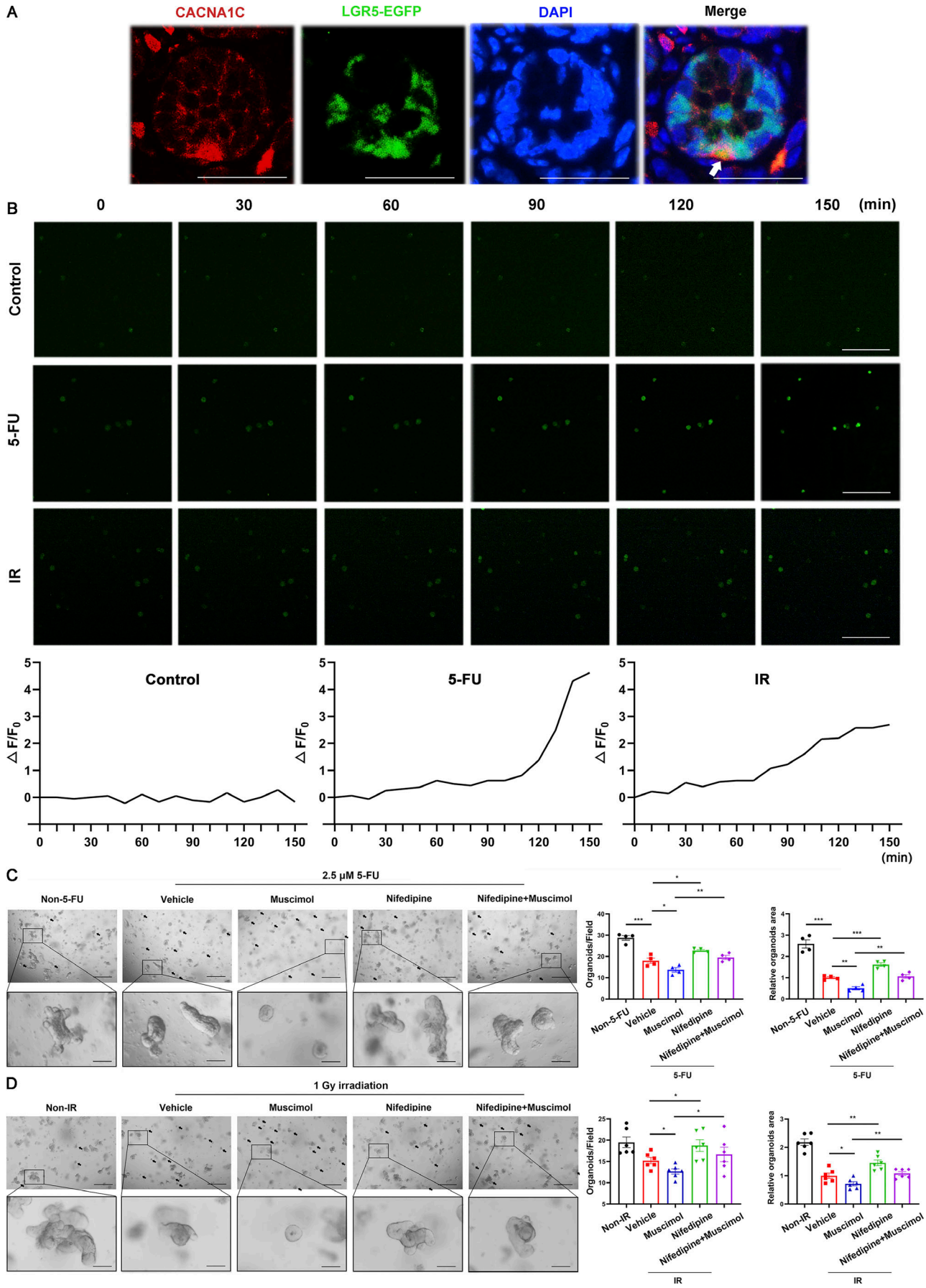

Figure 7. **Bicuculline inhibited L-type Ca^{2+} channels to regulate organoid survival. (A)** CACNA1C (red) and GFP (LGR5, green) immunofluorescence staining in intestinal crypts. Scale bar, 50 µm. Asterisks indicate CACNA1C $^{+}$/LGR5^{+} cell pairs. **(B)** Examination of the Fluo-4 AM fluorescent signal by confocal microscopy reflecting the variation of intracellular Ca^{2+} levels in mouse intestinal crypts after 5-FU or irradiation treatment. Scale bar, 100 µm. **(C and D)** Representative images of C57BL/6 mouse intestinal organoids 2 d after 5-FU (C) or irradiation treatment (D). Organoids were treated with vehicle, muscimol (1 µM), nifedipine (0.1 µM), or nifedipine (0.1 µM) + muscimol (1 µM). Scale bar, 500 µm (upper) or 100 µm (bottom). Arrows indicate dead organoids. In C and D, values are means ± SEM. *, P < 0.05; **, P < 0.01; and ***, P < 0.001 (two-tailed Student's *t* test). Data are representative of two (B) or three (A, C, and D) independent experiments.

were sacrificed 3 h after the final bicuculline treatment. Tumor volumes were measured with calipers and calculated as *volume* = (*length* × *width*^{2})/2 every 2 d.

Sample collection, histology, and immunostaining

The jejuna were surgically removed from the euthanized mice and flush-cleaned using PBS. Tissues were fixed in 4% paraformaldehyde, paraffin-embedded, and sectioned at 4 µm thickness for H&E staining and immunostaining. The sections were deparaffinized, sequentially rehydrated, and stained with H&E. For immunohistochemistry, rehydrated sections were treated with 10 ml of 30% H_2O_2 for 20 min at room temperature after being treated with 1× sodium citrate antigen retrieval solution for 20 min at 95°C. Sections were washed three times with PBS and incubated overnight at 4°C with the corresponding primary antibody diluted in a recommended antibody diluent. After the antibody solution was removed, the sections were washed three times with PBS for 5 min each. The sections were incubated for 30 min at room temperature with a secondary antibody. Diaminobenzidine was applied to each section and counterstained with hematoxylin for 2 min. Finally, each section was sequentially dehydrated and mounted with coverslips and neutral gum. For immunofluorescence, the rehydrated sections were treated with 0.1% Triton X-100 for 15 min and blocked with goat serum for 30 min. Slides were incubated with indicated antibodies at 4°C overnight. After washing with PBS, the sections were followed by incubation with secondary antibodies for 1 h at 37°C. DAPI was used for nuclear staining. Finally, each section was mounted using an antifade mounting medium. The detection target of each mouse was measured in a double-blind manner using two different photomicrographs. Measurements of villus length were from a minimum of 40 villi from different locations in the jejunum of each mouse. Measurements were taken from the top of the crypt to the tip of the villus using 100× H&E images. Positively stained cells were counted randomly in 40–50 crypts from different locations in the jejunum of each mouse. There were at least three different animals per group. The number of mice used in each experiment is indicated in the corresponding figure legend.

Isolation and treatment of mouse intestinal crypts

Mouse crypt isolation, organoid development, and passage were performed as described previously (Clevers, 2016). In detail, the mice were sacrificed and the intestinal segments were cut lengthwise. Then, the intestinal sheet was washed with Dulbecco PBS (DPBS) and cut into 2-mm pieces. All pieces were transferred into a 50-ml conical tube with 15 ml of cold DPBS and pipetted up and down three times. The rinsing procedure was repeated until the supernatant became clear. The tissue pieces were resuspended in 15 ml of 2 mM ethylenediaminetetraacetic acid and incubated at 4°C for 30 min. The tissue pieces were resuspended in 10 ml of cold DPBS and pipetted three times. The supernatant was filtered through a 70-µm filter and collected in a fresh 50-ml conical tube. After centrifugation at 300 *g* for 5 min at 4°C, the supernatant was poured off carefully. Freshly isolated crypts were cultured in IntestiCult Organoid Growth Medium (Mouse) from Stemcell Technologies.

Intestinal organoids were plated in 50 µl of Matrigel (356231; Corning) in 48-well plates 24 h before treatment with bicuculline (1 µM, S7071; Selleck) or muscimol (1 µM, 13667; Cayman Chemical). 5-FU (2.5 µM) or irradiation (1 Gy) treatment was administered 1 h later than drug treatment. For ATM inhibitor or L-type calcium channel blocker experiments, KU-60019 (1 µM, S1570; Selleck) or nifedipine (0.1 µM, N7634; Sigma-Aldrich) was used. Organoids ≥100 µm in diameter were enumerated 48 h after 5-FU or irradiation treatment. For detecting P53-dependent apoptosis, proteins were extracted from organoids 36 h after 5-FU treatment or 18 h after irradiation treatment. To detect the ATM-γ-H2AX axis, proteins were extracted from organoids 1 h after bicuculline treatment or 30 min after muscimol treatment. For the alkaline comet assay, individual cells were isolated from organoids 2 or 24 h after bicuculline or muscimol treatment in the absence of 5-FU or irradiation treatment, or 24 h after 5-FU treatment or 1 h after irradiation treatment. For 8-OHdG staining, organoids were collected 2 or 24 h after bicuculline or muscimol treatment in the absence of 5-FU or irradiation treatment, or 24 h after 5-FU treatment or 1 h after irradiation treatment.

Isolation of human colonic crypts

Isolation of healthy human colon crypts and organoid development were performed as previously described (Fujii et al., 2015). Surgically resected colonic tissues were obtained from the Qilu Hospital of Shandong University. The tissue samples were washed with 10 ml of ice-cold DPBS and minced thoroughly into the smallest pieces. Then, the tissue pieces were incubated with 10 ml of Gentle Cell Dissociation Reagent (100-0485; Stemcell Technologies) on a rocking platform set at 40 rpm for 30 min. After centrifugation at 290 *g* for 5 min, the supernatant was aspirated, and the tissue pieces were vigorously pipetted 20 times to isolate crypts with 1 ml of ice-cold DMEM+1% bovine serum albumin (BSA). The contents of the tube were passed through a 70-µm cell strainer into a new 15-ml conical tube. After centrifugation at 300 *g* for 5 min at 4°C, the supernatant was poured off carefully. Freshly isolated crypts were cultured in IntestiCult Organoid Growth Medium (Human) from Stemcell Technologies plus 10-µM Y-27632.

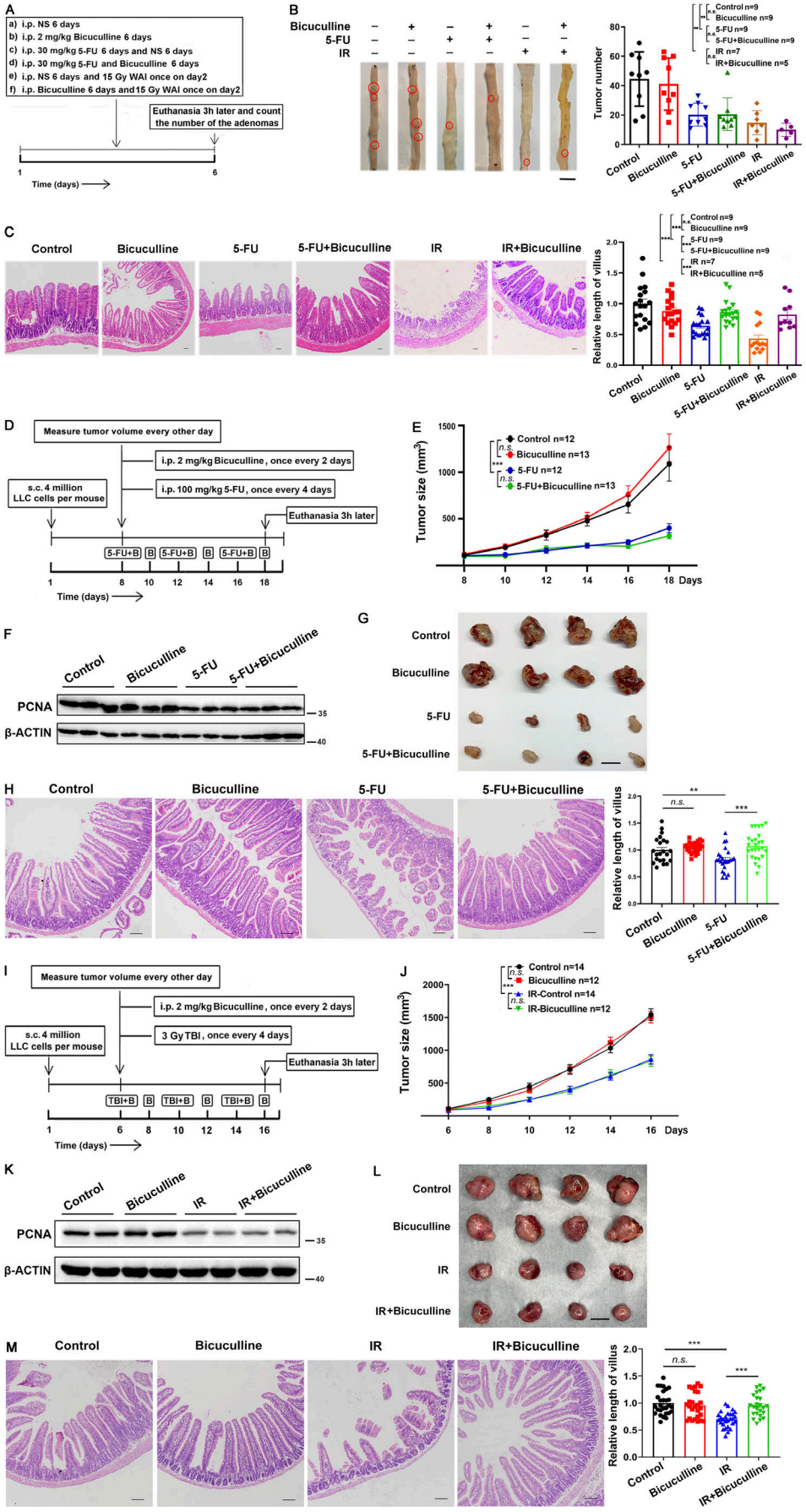

Figure 8. **Bicuculline protected the normal intestine in $Apc^{Min/+}$ or tumor-bearing mice from chemoradiotherapy without affecting antitumor activity. (A)** Schematic diagram of $Apc^{Min/+}$ mice treatment. **(B)** Representative image of adenomas in the small intestine from differently treated $Apc^{Min/+}$ mice. Scale bar, 1 cm. Histogram demonstrating the number of adenomas in the small intestine per mouse from A. **(C)** Representative images of H&E staining of the jejunum tissues. Scale bar, 100 µm. **(D)** Schematic diagram of tumor-bearing mice treatment with 5-FU. **(E)** Tumor sizes were measured every other day from days 8 to 18. **(F)** Immunoblot of PCNA in tumors from D at day 18. **(G)** Representative images of LLC tumors at day 18. Scale bar, 1 cm. **(H)** Representative images of H&E staining of the jejunum tissues. Scale bar, 100 µm. **(I)** Schematic diagram of tumor-bearing mice treatment with irradiation. **(J)** Tumor sizes were measured every other day from days 6 to 16. **(K)** Immunoblot of PCNA in tumors from I at day 16. **(L)** Representative images of LLC tumors at day 16. Scale bar, 1 cm. **(M)** Representative images of H&E staining of the jejunum tissues. Scale bar, 100 µm. In E and J values are means ± SEM; *n* = indicated mice per group. n.s., not significant; ***, P < 0.001 (ANOVA). In B, C, H, and M, values are means ± SEM; *n* = indicated mice per group. n.s., not significant; **, P < 0.01; and ***, P < 0.001 (two-tailed Student's *t* test). Data are representative of two (E–H and J–M) or four (B and C) independent experiments. Source data are available for this figure: SourceData F8.

Colonic organoids were plated in 25 µl of Matrigel (356231; Corning) and 25 µl of advanced DMEM/F-12 with 15-mM HEPES plus 5% BSA in 48-well plates 24 h before treatment with flumazenil (1 µM, S1332; Selleck). 5-FU (2.5 µM) or irradiation (1 Gy) was administered 1 h after flumazenil treatment. Organoids ≥100 µm in diameter were enumerated 48 h after 5-FU or irradiation treatment. All participants provided written informed consent, and the use of human tissues was approved by the Medical Institutional Ethics Committee of Qilu Hospital, Shandong University, China (KYLL-202011-209-01).

Alcian blue-periodic acid Schiff's (AB-PAS) staining

For the detection of acidic mucin, AB-PAS staining of paraffin-embedded tissue sections was performed using a commercial AB-PAS kit. The sections were fixated, dehydrated, and embedded; placed in periodic acid solution; and left at room temperature for 10 min. Then, the samples were placed in a Schiff reagent and placed in a dark place at room temperature for 15 min. Finally, the samples were rinsed in tap water for 10 min and placed in a hematoxylin staining solution for 2 min. AB-PAS–positive cells were counted randomly in 40–50 villi from different locations in the jejunum of each mouse.

Protein extraction and Western blotting

Intestinal tissues, tumor tissues, and organoid samples from each group were lysed by adding a 1× SDS sample buffer and sonicating for 10 min. A 2× loading buffer was added to the sample and heated to 100°C for 5 min. Protein extracts were isolated, separated by SDS polyacrylamide, and transferred to a polyvinylidene difluoride membrane. The membrane was incubated overnight with specific primary antibodies at 4°C. Then, it was incubated with the Enhanced Chemiluminescence Detection Kit and determined using a chemiluminescence detection system. Band density was determined using Image J analyzer software. The antibodies used in this study are listed in Table S1.

Real-time PCR (RT-PCR)

All mouse RT-PCR primer pairs were purchased from Beijing Genomics Institute. Intestinal tissues were surgically removed from euthanized mice and flush-cleaned using PBS. Total mRNA was extracted according to the instructions of the RNA extraction kit (RN2802; Aidlab Biotechnologies). Total isolated mRNAs were reverse-transcribed to cDNA using HiScript III RT SuperMix (R323-01; Vazyme Biotech). Finally, the StepOnePlus Real-Time PCR System (4376600; Thermo Fisher Scientific) was used to detect fluorescence intensity. The adjusted amounts of total cDNA were used as starting materials in identical quantities for the purpose of comparison. Primers used in this study are listed in Table S2.

Immunofluorescence analysis of 8-OHdG

Organoids subjected to indicated treatments were collected and washed with DPBS. After attachment to adhesive slides, organoids were fixed with 4% paraformaldehyde for 30 min at 4°C, washed with PBS, and treated with 0.1% Triton X-100 for 15 min. Next, organoids were blocked with goat serum for 30 min and incubated with the 8-OHdG antibody at 4°C overnight. After washing with PBS, the sections were followed by incubation with a secondary antibody for 1 h at 37°C. The DAPI was used for nuclear staining. Finally, each section was mounted using an antifade mounting medium.

Alkaline comet assay

Organoids were performed according to the previous description (Olive and Banath, 2006). Briefly, individual cells were isolated from organoids with the indicated treatments and suspended in low melting agarose. After lysis in the Comet Assay Lysis Solution (4250-050-01; R&D System) for 2 h, the mixture was separated by electrophoresis under alkaline conditions at 17 V for 20 min. Gel Green was used for nucleic acid staining. Data were collected with a fluorescent microscope and analyzed using CASP software.

Ca^{2+} measurements

Intracellular Ca^{2+} levels were monitored using the Fluo-4 AM fluorescent indicator. Briefly, 2-µM Fluo-4 AM Ca^{2+} probe was added to cells 30 min prior to 5-FU or irradiation treatment. Time-lapse analysis of living cells was performed using a Zeiss LSM780 laser confocal microscope. Quantification of fluorescence intensity was performed using ImageJ software (Vila Cuenca et al., 2021).

Cell lines and treatment

LLC and MC-38 cells were maintained at 37°C and 5% CO_2 in the RPMI 1640 medium supplemented with 10% fetal bovine serum, penicillin (100 U/ml), and streptomycin (100 µg/ml).

Cell proliferation assay

LLC and HT-29 cells (3×10^3 cells/well) were seeded in the 96-well plates and cultivated overnight. Then, 10-µl cell counting kit-8 (CCK-8) solution was added to each well of the plate and

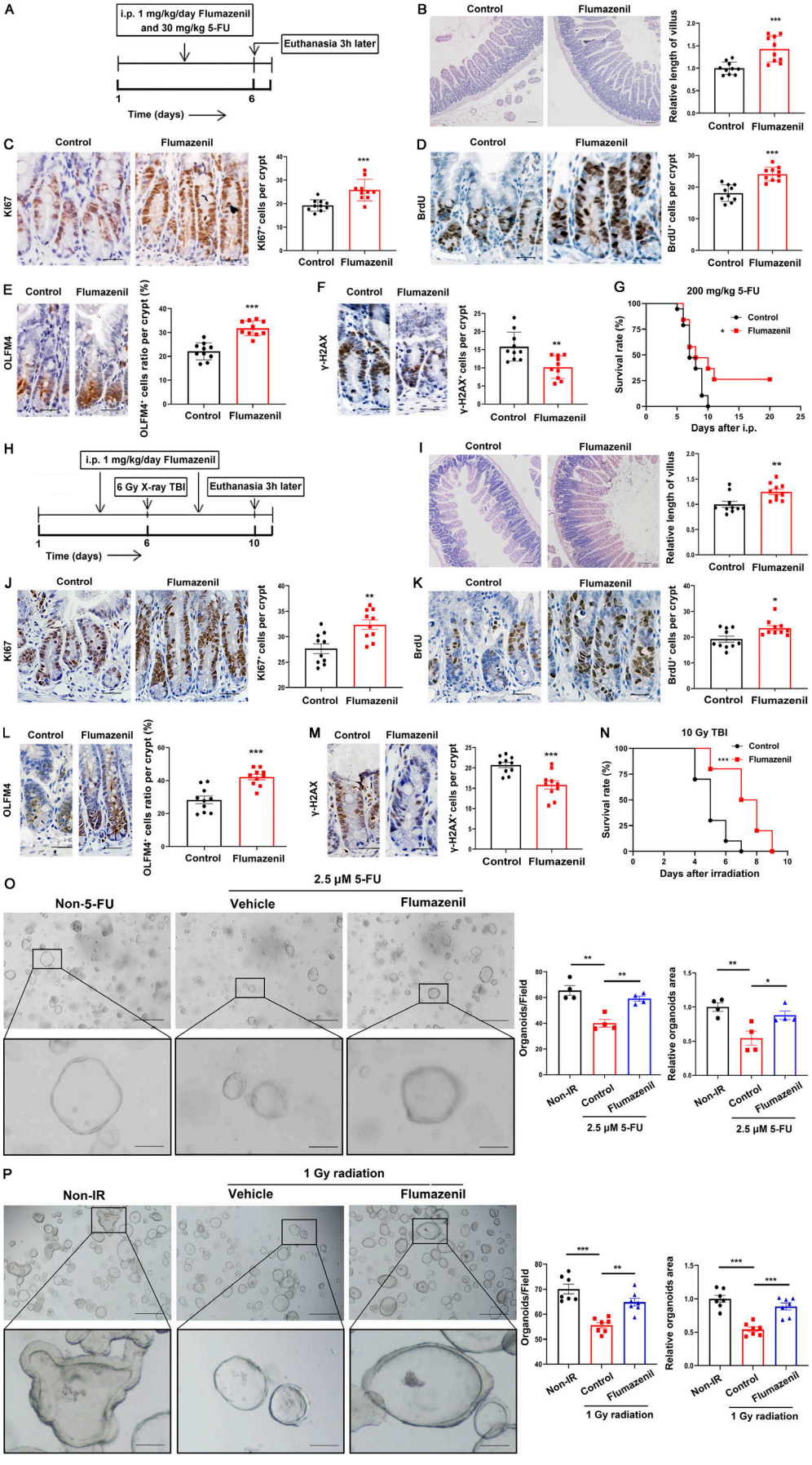

Figure 9. **Flumazenil protected against 5-FU– or irradiation-induced IEC apoptosis.** WT mice were treated with 5-FU (30 mg/kg, i.p., 6 d) or irradiation (6 Gy, TBI, once) with or without flumazenil (1 mg/kg, i.p.) treatment. For survival analysis, mice were treated with 5-FU (200 mg/kg, i.p.) or irradiation (10 Gy, TBI) once. **(A)** Schematic diagram of 5-FU treatment to C57BL/6 mice. **(B)** Representative images of H&E staining of the jejunum tissues from mice treated as in A. Scale bar, 100 µm. **(C–F)** Representative images of KI67 (C), BrdU (D), OLFM4 (E), and γ-H2AX (F) staining in the jejunum tissues from mice treated as in A. Scale bar, 50 µm. **(G)** Log-rank (Mantel-Cox) survival analysis of mice treated with or without flumazenil after 5-FU treatment on day 0. n = 19 mice per group; *, P < 0.05 (log-rank [Mantel-Cox] test). **(H)** Schematic diagram of irradiation treatment to C57BL/6 mice. **(I)** Representative images of H&E staining of the jejunum tissues from mice treated as in H. Scale bar, 100 µm. **(J–M)** Representative images of KI67 (J), BrdU (K), OLFM4 (L), and γ-H2AX (M) staining of the jejunum tissues from mice treated as in H. Scale bar, 50 µm. **(N)** Log-rank (Mantel-Cox) survival analysis of mice treated with or without flumazenil after irradiation treatment on day 0. n = 10 mice per group; ***, P < 0.001 (log-rank [Mantel-Cox] test). **(O and P)** Representative images of human colonic organoids treated with vehicle or flumazenil (1 µM) 2 d after 5-FU (2.5 µM; O) or irradiation (1 Gy) treatment (P). Scale bar, 500 µm (upper) or 100 µm (bottom). In B–F, and I–M, values are means ± SEM; n = 5 mice per group. *, P < 0.05; **, P < 0.01; and ***, P < 0.001 (two-tailed Student's t test). In O and P, values are means ± SEM. *, P < 0.05; **, P < 0.01; and ***, P < 0.001 (two-tailed Student's t test). Data are representative of two (B–G and I–N) or three (O and P) independent experiments.

incubated for 2 h. A microplate reader was used to measure the absorbance at 450 nm.

Database

The expression profile of *Gabra1* RNA-seq data for 620 colon adenocarcinoma (COAD) patients was obtained from TCGA data portal (https://tcga-data.nci.nih.gov/tcga/), and 51 of the tumors also had mRNA expression data of paired normal tissue samples. Besides, *Gabra1* RNA-seq data of 779 normal colon tissue samples were downloaded from the GTEx database (https://www.gtexportal.org/). All the above analysis methods and R package were implemented by R foundation for statistical computing (2020) version 4.0.3.

Statistical analysis

All data are represented as the mean ± SEM, unless otherwise indicated. Statistical analysis was performed using a two-tailed Student's t test to compare data between two groups. To compare data between three or more groups, ANOVA was performed, followed by the Student–Newman–Keuls's post hoc test for pairwise comparisons. Survival rates were analyzed using the log-rank (Mantel-Cox) test. Statistical significance was determined as P values <0.05. n.s., not significant; *, P < 0.05; **, P < 0.01; and ***, P < 0.001.

Online supplemental material

Fig. S1 shows that the loss of *Gabra1* in IECs had no effect on the physiological phenotype of the intestine in mice. Fig. S2 shows that bicuculline protected against 5-FU– or irradiation-induced intestinal injury in mice. Fig. S3 shows that bicuculline or muscimol had no effect on ROS or DNA damage in organoids in the absence of 5-FU or irradiation treatment. Fig. S4 shows that bicuculline protected the normal intestine of MC38 tumor-bearing mice from fractionated abdominal radiotherapy without affecting its antitumor activity. Fig. S5 shows that bicuculline or muscimol did not affect tumor cell line proliferation. Table S1 lists antibodies used in this study. Table S2 lists the primers used for RT-PCR analysis.

Acknowledgments

Special thanks go to Prof. Junhui Zhen from the Pathology Department of Qilu Hospital for providing small intestine samples from normal people.

This work was supported by grants from the National Natural Science Foundation of China (31971061, 81903087) and Taishan Pandeng Scholar Program of Shandong Province (tspd20210321).

Author's contributions: C. Zhang performed research, analyzed the data, and wrote the manuscript; Y. Zhou, J. Zheng and N. Ning performed research and analyzed the data; H. Liu, W. Jiang, X. Yu and Y. Li performed research; K. Mu, W. Guo and H. Hu provided materials; J. Li conceptualized the project and funded the work; D. Chen was responsible for the design of the study, interpretation of data, and writing of the manuscript.

Disclosures: C. Zhang reported a patent to CN202210946395.9 pending. J. li reported a patent to CN202210946395.9 pending. D. Chen reported a patent to CN202210946395.9 pending. No other disclosures were reported.

Submitted: 26 March 2022
Revised: 7 August 2022
Accepted: 26 August 2022

References

Accarie, A., B. I'Homme, M.A. Benadjaoud, S.K. Lim, C. Guha, M. Benderitter, R. Tamarat, and A. Semont. 2020. Extracellular vesicles derived from mesenchymal stromal cells mitigate intestinal toxicity in a mouse model of acute radiation syndrome. *Stem Cell Res. Ther.* 11:371. https://doi.org/10.1186/s13287-020-01887-1

Andang, M., J. Hjerling-Leffler, A. Moliner, T.K. Lundgren, G. Castelo-Branco, E. Nanou, E. Pozas, V. Bryja, S. Halliez, H. Nishimaru, et al. 2008. Histone H2AX-dependent GABA(A) receptor regulation of stem cell proliferation. *Nature*. 451:460–U464. https://doi.org/10.1038/nature06488

Andreyev, H.J. 2016. GI consequences of cancer treatment: A clinical perspective. *Radiat. Res.* 185:341–348. https://doi.org/10.1667/RR14272.1

Auteri, M., M.G. Zizzo, and R. Serio. 2015. GABA and GABA receptors in the gastrointestinal tract: From motility to inflammation. *Pharmacol. Res.* 93:11–21. https://doi.org/10.1016/j.phrs.2014.12.001

Bakkenist, C.J., and M.B. Kastan. 2003. DNA damage activates ATM through intermolecular autophosphorylation and dimer dissociation. *Nature*. 421:499–506. https://doi.org/10.1038/nature01368

Barker, N., A. van Oudenaarden, and H. Clevers. 2012. Identifying the stem cell of the intestinal crypt: Strategies and pitfalls. *Cell Stem Cell*. 11:452–460. https://doi.org/10.1016/j.stem.2012.09.009

Berger, M.E., D.M. Christensen, P.C. Lowry, O.W. Jones, and A.L. Wiley. 2006. Medical management of radiation injuries: Current approaches. *Occup. Med.* 56:162–172. https://doi.org/10.1093/occmed/kql011

Bjurström, H., J. Wang, I. Ericsson, M. Bengtsson, Y. Liu, S. Kumar-Mendu, S. Issazadeh-Navikas, and B. Birnir. 2008. GABA, a natural immunomodulator

of T lymphocytes. *J. Neuroimmunol.* 205:44–50. https://doi.org/10.1016/j.jneuroim.2008.08.017

Brogden, R.N., and K.L. Goa. 1991. Flumazenil: A reappraisal of its pharmacological properties and therapeutic efficacy as a benzodiazepine antagonist. *Drugs.* 42:1061–1089. https://doi.org/10.2165/00003495-199142060-00010

Can, G., B. Akpinar, Y. Baran, B. Zhivotovsky, and M. Olsson. 2013. 5-Fluorouracil signaling through a calcium-calmodulin-dependent pathway is required for p53 activation and apoptosis in colon carcinoma cells. *Oncogene.* 32:4529–4538. https://doi.org/10.1038/onc.2012.467

Chen, L., F. Liao, Z. Jiang, C. Zhang, Z. Wang, P. Luo, Q. Jiang, J. Wu, Q. Wang, M. Luo, et al. 2020. Metformin mitigates gastrointestinal radiotoxicity and radiosensitises P53 mutation colorectal tumours via optimising autophagy. *Br. J. Pharmacol.* 177:3991–4006. https://doi.org/10.1111/bph.15149

Clevers, H. 2016. Modeling development and disease with organoids. *Cell.* 165:1586–1597. https://doi.org/10.1016/j.cell.2016.05.082

Vila Cuenca, M., A. Cochrane, F.E. van den Hil, A.A.F. de Vries, S.A.J. Oberstein, C.L. Mummery, and V.V. Orlova. 2021. Engineered 3D vessel-on-chip using hiPSC-derived endothelial- and vascular smooth muscle cells. *Stem Cell Rep.* 16:2159–2168. https://doi.org/10.1016/j.stemcr.2021.08.003

D'Andrea, G.M. 2005. Use of antioxidants during chemotherapy and radiotherapy should be avoided. *CA Cancer J. Clin.* 55:319–321. https://doi.org/10.3322/canjclin.55.5.319

Dey, D.K., S.N. Chang, Y. Vadlamudi, J.G. Park, and S.C. Kang. 2020. Synergistic therapy with tangeretin and 5-fluorouracil accelerates the ROS/JNK mediated apoptotic pathway in human colorectal cancer cell. *Food Chem. Toxicol.* 143:111529. https://doi.org/10.1016/j.fct.2020.111529

Dubois, A., and R.I. Walker. 1988. Prospects for management of gastrointestinal injury associated with the acute radiation syndrome. *Gastroenterology.* 95:500–507. https://doi.org/10.1016/0016-5085(88)90512-4

Shao, L., A. Elujoba-Bridenstine, K.E. Zink, L.M. Sanchez, B.J.Cox, K.E.Pollok, A.L. Sinn, B.J. Bailey, E.C. Sims, S.H. Cooper, et al. 2021. The neurotransmitter receptor Gabbr1 regulates proliferation and function of hematopoietic stem and progenitor cells. *Blood.* 137:775–787. https://doi.org/10.1182/blood.2019004415

Erlandsson, J., T. Holm, D. Pettersson, A. Berglund, B. Cedermark, C. Radu, H. Johansson, M. Machado, F. Hjern, O. Hallbook, et al. 2017. Optimal fractionation of preoperative radiotherapy and timing to surgery for rectal cancer (stockholm III): A multicentre, randomised, non-blinded, phase 3, non-inferiority trial. *Lancet Oncol.* 18:336–346. https://doi.org/10.1016/S1470-2045(17)30086-4

Erlitzki, R., Y. Gong, M. Zhang, and G. Minuk. 2000. Identification of gamma-aminobutyric acid receptor subunit types in human and rat liver. *Am. J. Physiol. Gastrointest. Liver Physiol.* 279:G733–G739. https://doi.org/10.1152/ajpgi.2000.279.4.G733

Fujii, M., M. Matano, K. Nanki, and T. Sato. 2015. Efficient genetic engineering of human intestinal organoids using electroporation. *Nat. Protoc.* 10:1474–1485. https://doi.org/10.1038/nprot.2015.088

Gregorieff, A., Y. Liu, M.R. Inanlou, Y. Khomchuk, and J.L. Wrana. 2015. Yap-dependent reprogramming of Lgr5(+) stem cells drives intestinal regeneration and cancer. *Nature.* 526:715–718. https://doi.org/10.1038/nature15382

Gudkov, A.V., and E.A. Komarova. 2010. Radioprotection: Smart games with death. *J. Clin. Invest.* 120:2270–2273. https://doi.org/10.1172/JCI43794

Guleria, A., and S. Chandna. 2016. ATM kinase: Much more than a DNA damage responsive protein. *DNA Repair.* 39:1–20. https://doi.org/10.1016/j.dnarep.2015.12.009

Guleria, A., N. Thukral, and S. Chandna. 2018. Intrinsic attenuation of post-irradiation calcium and ER stress imparts significant radioprotection to lepidopteran insect cells. *Biochem. Biophys. Res. Commun.* 498:905–911. https://doi.org/10.1016/j.bbrc.2018.03.078

Hauer-Jensen, M., J.W. Denham, and H.J.N. Andreyev. 2014. Radiation enteropathy-pathogenesis, treatment and prevention. *Nat. Rev. Gastroenterol. Hepatol.* 11:470–479. https://doi.org/10.1038/nrgastro.2014.46

Hendry, J.H., and K. Otsuka. 2016. The role of gene mutations and gene products in intestinal tissue reactions from ionising radiation. *Mutat. Res. Rev. Mutat. Res.* 770:328–339. https://doi.org/10.1016/j.mrrev.2016.07.006

Jin, Z., S.K. Mendu, and B. Birnir. 2013. GABA is an effective immunomodulatory molecule. *Amino Acids.* 45:87–94. https://doi.org/10.1007/s00726-011-1193-7

Johnstone, V.P., and L.C. Hool. 2014. Glutathionylation of the L-type Ca^{2+} channel in oxidative stress-induced pathology of the heart. *Int. J. Mol. Sci.* 15:19203–19225. https://doi.org/10.3390/ijms151019203

Keefe, D.M., J. Brealey, G.J. Goland, and A.G. Cummins. 2000. Chemotherapy for cancer causes apoptosis that precedes hypoplasia in crypts of the small intestine in humans. *Gut.* 47:632–637. https://doi.org/10.1136/gut.47.5.632

Kim, J.K., Y.S. Kim, H.M. Lee, H.S. Jin, C. Neupane, S. Kim, S.H. Lee, J.J. Min, M. Sasai, J.H. Jeong, et al. 2018. GABAergic signaling linked to autophagy enhances host protection against intracellular bacterial infections. *Nat. Commun.* 9:4184. https://doi.org/10.1038/s41467-018-06487-5

Kim, K.A., M. Kakitani, J. Zhao, T. Oshima, T. Tang, M. Binnerts, Y. Liu, B. Boyle, E. Park, P. Emtage, et al. 2005. Mitogenic influence of human R-spondin1 on the intestinal epithelium. *Science.* 309:1256–1259. https://doi.org/10.1126/science.1112521

Lee, S.Y., E.K. Jeong, M.K. Ju, H.M. Jeon, M.Y. Kim, C.H. Kim, H.G. Park, S.I. Han, and H.S. Kang. 2017. Induction of metastasis, cancer stem cell phenotype, and oncogenic metabolism in cancer cells by ionizing radiation. *Mol. Cancer.* 16:10. https://doi.org/10.1186/s12943-016-0577-4

Leibowitz, B.J., L. Yang, L. Wei, M.E. Buchanan, M. Rachid, R.A. Parise, J.H. Beumer, J.L. Eiseman, R.E. Schoen, L. Zhang, and J. Yu. 2018. Targeting p53-dependent stem cell loss for intestinal chemoprotection. *Sci. Transl. Med.* 10:eaam7610. https://doi.org/10.1126/scitranslmed.aam7610

Liu, X., Q. Wang, T.F. Haydar, and A. Bordey. 2005. Nonsynaptic GABA signaling in postnatal subventricular zone controls proliferation of GFAP-expressing progenitors. *Nat. Neurosci.* 8:1179–1187. https://doi.org/10.1038/nn1522

Liu, Z., H. Tian, J. Jiang, Y. Yang, S. Tan, X. Lin, H. Liu, and B. Wu. 2016. β-Arrestin-2 modulates radiation-induced intestinal crypt progenitor/stem cell injury. *Cell Death Differ.* 23:1529–1541. https://doi.org/10.1038/cdd.2016.38

Lu, W., Y. Xie, B. Huang, T. Ma, H. Wang, B. Deng, S. Zou, W. Wang, Q. Tang, Z. Yang, et al. 2021. Platelet-derived growth factor C signaling is a potential therapeutic target for radiation proctopathy. *Sci. Transl. Med.* 13:eabc2344. https://doi.org/10.1126/scitranslmed.abc2344

Ma, X., Q. Sun, X. Sun, D. Chen, C. Wei, X. Yu, C. Liu, Y. Li, and J. Li. 2018. Activation of GABA(A) receptors in colon epithelium exacerbates acute colitis. *Front. Immunol.* 9:987. https://doi.org/10.3389/fimmu.2018.00987

Mirzayans, R., B. Andrais, A. Scott, and D. Murray. 2012. New insights into p53 signaling and cancer cell response to DNA damage: Implications for cancer therapy. *J. Biomed. Biotechnol.* 2012:170325. https://doi.org/10.1155/2012/170325

Moss, R.W. 2007. Do antioxidants interfere with radiation therapy for cancer? *Integr. Cancer Ther.* 6:281–292. https://doi.org/10.1177/1534735407305655

Niu, G., L. Deng, X. Zhang, Z. Hu, S. Han, K. Xu, R. Hong, H. Meng, and C. Ke. 2020. GABRD promotes progression and predicts poor prognosis in colorectal cancer. *Open Med.* 15:1172–1183. https://doi.org/10.1515/med-2020-0128

Olive, P.L., and J.P. Banath. 2006. The comet assay: A method to measure DNA damage in individual cells. *Nat. Protoc.* 1:23–29. https://doi.org/10.1038/nprot.2006.5

Olivier, M., M. Hollstein, and P. Hainaut. 2010. TP53 mutations in human cancers: Origins, consequences, and clinical use. *Cold Spring Harbor Perspect. Biol.* 2:a001008. https://doi.org/10.1101/cshperspect.a001008

Olsen, R.W., and W. Sieghart. 2008. International union of pharmacology. LXX. Subtypes of gamma-aminobutyric Acid(A) receptors: Classification on the basis of subunit composition, pharmacology, and function. Update. *Pharmacol. Rev.* 60:243–260. https://doi.org/10.1124/pr.108.00505

Qiu, W., B. Leibowitz, L. Zhang, and J. Yu. 2010. Growth factors protect intestinal stem cells from radiation-induced apoptosis by suppressing PUMA through the PI3K/AKT/p53 axis. *Cancer Res.* 70. https://doi.org/10.1158/1538-7445.am10-3198

Roberts, E., and S. Frankel. 1950. Gamma-aminobutyric acid in brain: Its formation from glutamic acid. *J. Biol. Chem.* 187:55–63. https://doi.org/10.1016/s0021-9258(19)50929-2

Roth, F.C., and A. Draguhn. 2012. GABA metabolism and transport: Effects on synaptic efficacy. *Neural Plast.* 2012:805830. https://doi.org/10.1155/2012/805830

Seifi, M., S. Rodaway, U. Rudolph, and J.D. Swinny. 2018. GABA(A) receptor subtypes regulate stress-induced colon inflammation in mice. *Gastroenterology.* 155:852–864.e3. https://doi.org/10.1053/j.gastro.2018.05.033

Shu, Q., J. Liu, X. Liu, S. Zhao, H. Li, Y. Tan, and J. Xu. 2016. GABAB R/GSK-3β/NF-κB signaling pathway regulates the proliferation of colorectal cancer cells. *Cancer Med.* 5:1259–1267. https://doi.org/10.1002/cam4.686

Siddiqui, M.S., M. Francois, M.F. Fenech, and W.R. Leifert. 2015. Persistent gamma H2AX: A promising molecular marker of DNA damage and aging. *Mutat. Res. Rev. Mutat. Res.* 766:1–19. https://doi.org/10.1016/j.mrrev.2015.07.001

Smith, T.A., D.R. Kirkpatrick, S. Smith, T.K. Smith, T. Pearson, A. Kailasam, K.Z. Herrmann, J. Schubert, and D.K. Agrawal. 2017. Radioprotective agents to prevent cellular damage due to ionizing radiation. *J. Transl. Med.* 15:232. https://doi.org/10.1186/s12967-017-1338-x

Valenzuela, C.F., A. Kazlauskas, S.J. Brozowski, J.L. Weiner, K.A. Demali, B.J. McDonald, S.J. Moss, T.V. Dunwiddie, and R.A. Harris. 1995. Platelet-derived growth factor receptor is a novel modulator of type A gamma-aminobutyric acid-gated ion channels. *Mol. Pharmacol.* 48:1099–1107

Yu, J. 2013. Intestinal stem cell injury and protection during cancer therapy. *Transl. Cancer Res.* 2:384–396

Zhang, S., Y. Liu, D. Xiang, J. Yang, D. Liu, X. Ren, and C. Zhang. 2018. Assessment of dose-response relationship of 5-fluorouracil to murine intestinal injury. *Biomed. Pharmacother.* 106:910–916. https://doi.org/10.1016/j.biopha.2018.07.029

Zheng, Z., X. Zhang, J. Liu, P. He, S. Zhang, Y. Zhang, J. Gao, S. Yang, N. Kang, M.I. Afridi, et al. 2021. GABAergic synapses suppress intestinal innate immunity via insulin signaling in Caenorhabditis elegans. *Proc. Natl. Acad. Sci. USA.* 118:e2021063118. https://doi.org/10.1073/pnas.2021063118

Zhou, W.J., Z.H. Geng, J.R. Spence, and J.G. Geng. 2013. Induction of intestinal stem cells by R-spondin 1 and Slit2 augments chemoradioprotection. *Nature.* 501:107–111. https://doi.org/10.1038/nature12416

Zhu, F., M. Feng, R. Sinha, M.P. Murphy, F. Luo, K.S. Kao, K. Szade, J. Seita, and I.L. Weissman. 2019. The GABA receptor GABRR1 is expressed on and functional in hematopoietic stem cells and megakaryocyte progenitors. *Proc. Natl. Acad. Sci. USA.* 116:18416–18422. https://doi.org/10.1073/pnas.1906251116

Supplemental material

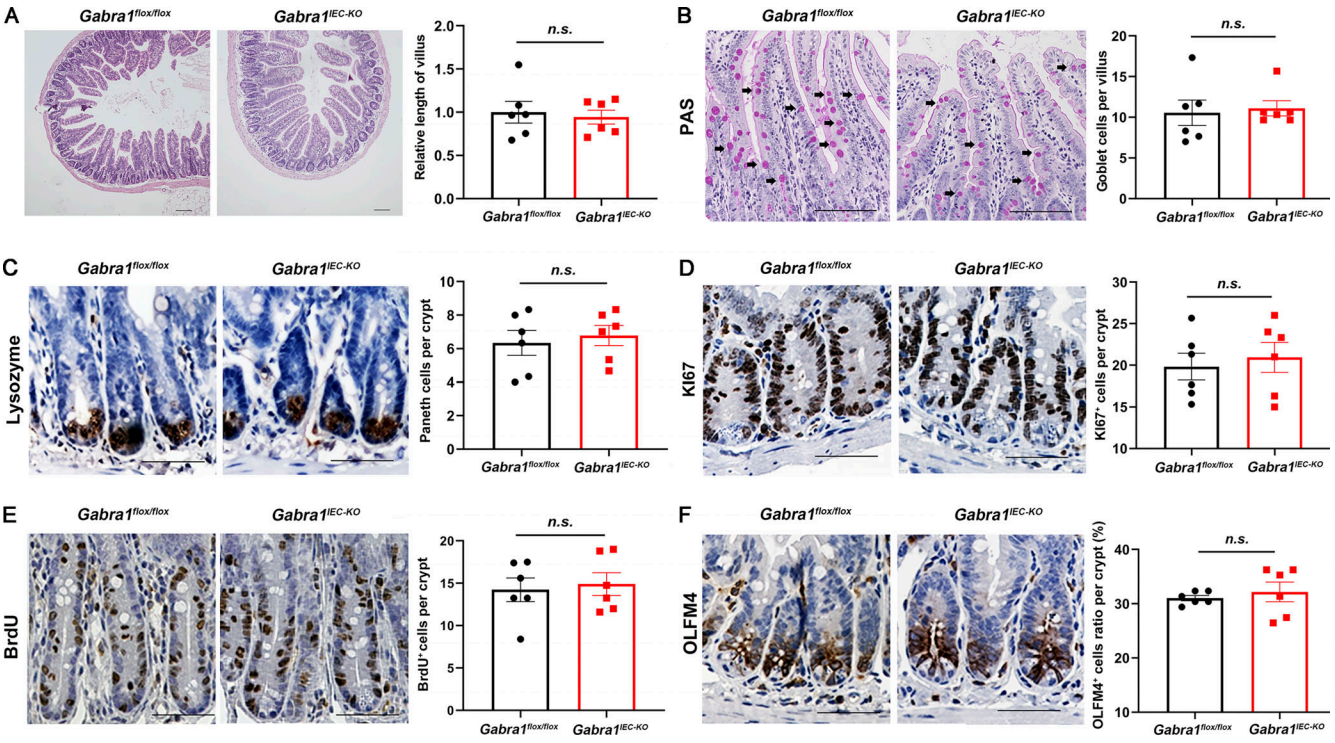

Figure S1. **Loss of *Gabra1* in IECs had no effect on the physiological phenotype of the intestine in mice.** The jejunum tissues from 8-wk-old *Gabra1*$^{IEC\text{-}KO}$ mice and their littermate control mice (*Gabra1*$^{flox/flox}$) were obtained and analyzed for indicated phenotype. **(A)** Representative images of H&E staining of the jejunum tissues. Scale bar, 100 µm. **(B–F)** Representative images of PAS (B), lysozyme (C), KI67 (D), BrdU (E), and OLFM4 (F) stained of the jejunum tissues. Scale bar, 100 µm. In A–F, values are means ± SEM; *n* = 3 mice per group. n.s., not significant (two-tailed Student's *t* test). In B, arrows indicate goblet cells. Data are representative of at least three (A–F) independent experiments.

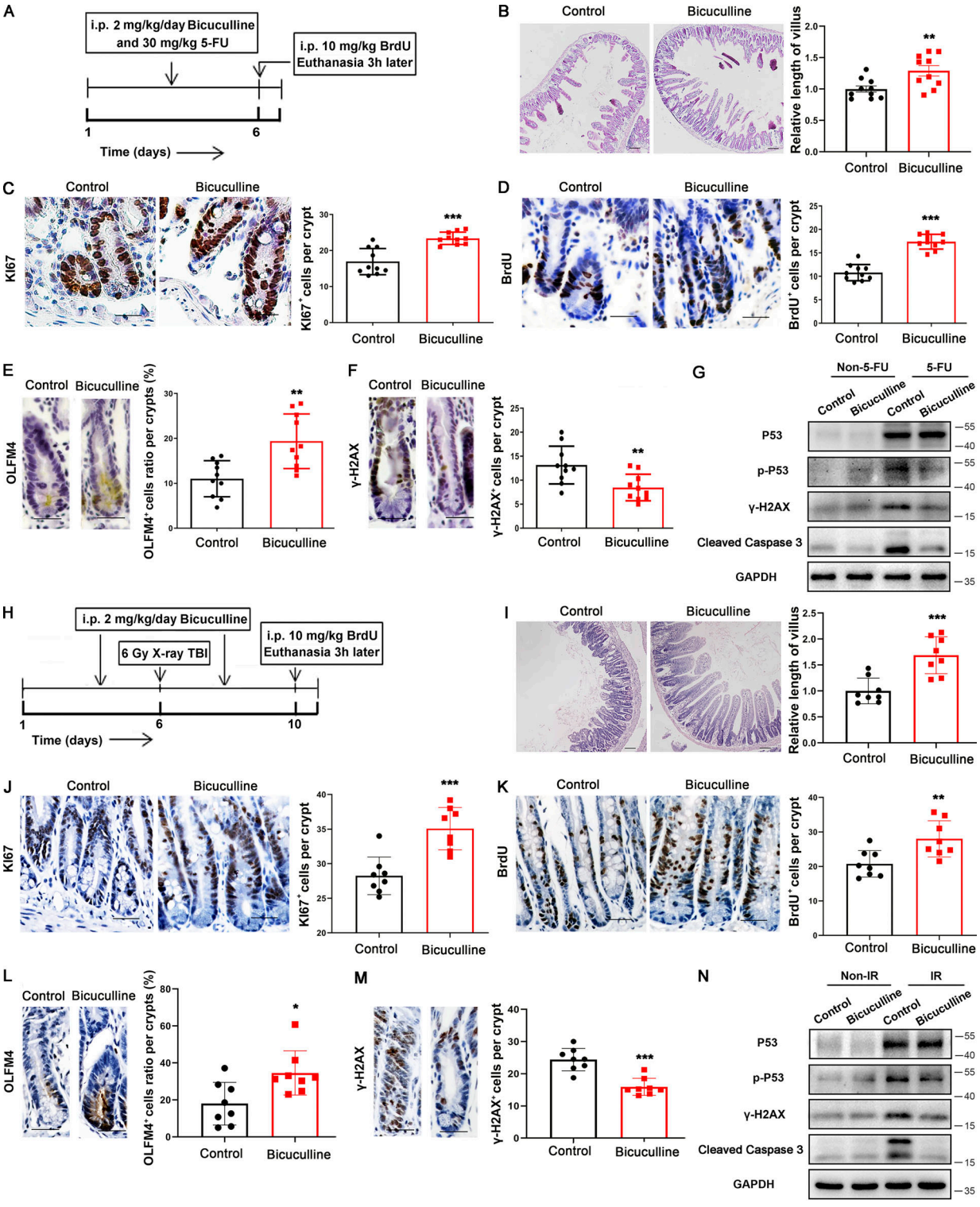

Figure S2. **Bicuculline protected against 5-FU- or irradiation-induced intestinal injury in mice.** Mice were treated with 5-FU (30 mg/kg, i.p., 6 d) or irradiation (6 Gy, TBI, once) with or without bicuculline (2 mg/kg, i.p.) treatment. **(A)** Schematic diagram of 5-FU treatment to C57BL/6 mice. **(B)** Representative images of H&E staining of the jejunum tissues from mice treated as in A. Scale bar, 100 µm. **(C–F)** Representative images of KI67 (C), BrdU (D), OLFM4 (E), and γ-H2AX (F) staining of the jejunum tissues from mice treated as in A. Scale bar, 50 µm. **(G)** Immunoblots of P53, p-P53, γ-H2AX, and Cleaved Caspase 3 in intestinal mucosa from mice treated as in A. In B–F, values are means ± SEM; n = 5 mice per group. **, P < 0.01; and ***, P < 0.001 (two-tailed Student's t test). **(H)** Schematic diagram of irradiation treatment to C57BL/6 mice. **(I)** Representative images of H&E staining of the jejunum tissues from mice treated as in H. Scale bar, 100 µm. **(J–M)** Representative images of KI67 (J), BrdU (K), OLFM4 (L), and γ-H2AX (M) staining of the jejunum tissues from mice treated as in H. Scale bar, 50 µm. **(N)** Immunoblots of P53, p-P53, γ-H2AX, and Cleaved Caspase 3 in intestinal mucosa from mice treated as in H. In I–M, values are means ± SEM; n = 4 mice per group. *, P < 0.05; **, P < 0.01; and ***, P < 0.001 (two-tailed Student's t test). Data are representative of at least three (B–G and I–N) independent experiments. Source data are available for this figure: SourceData FS2.

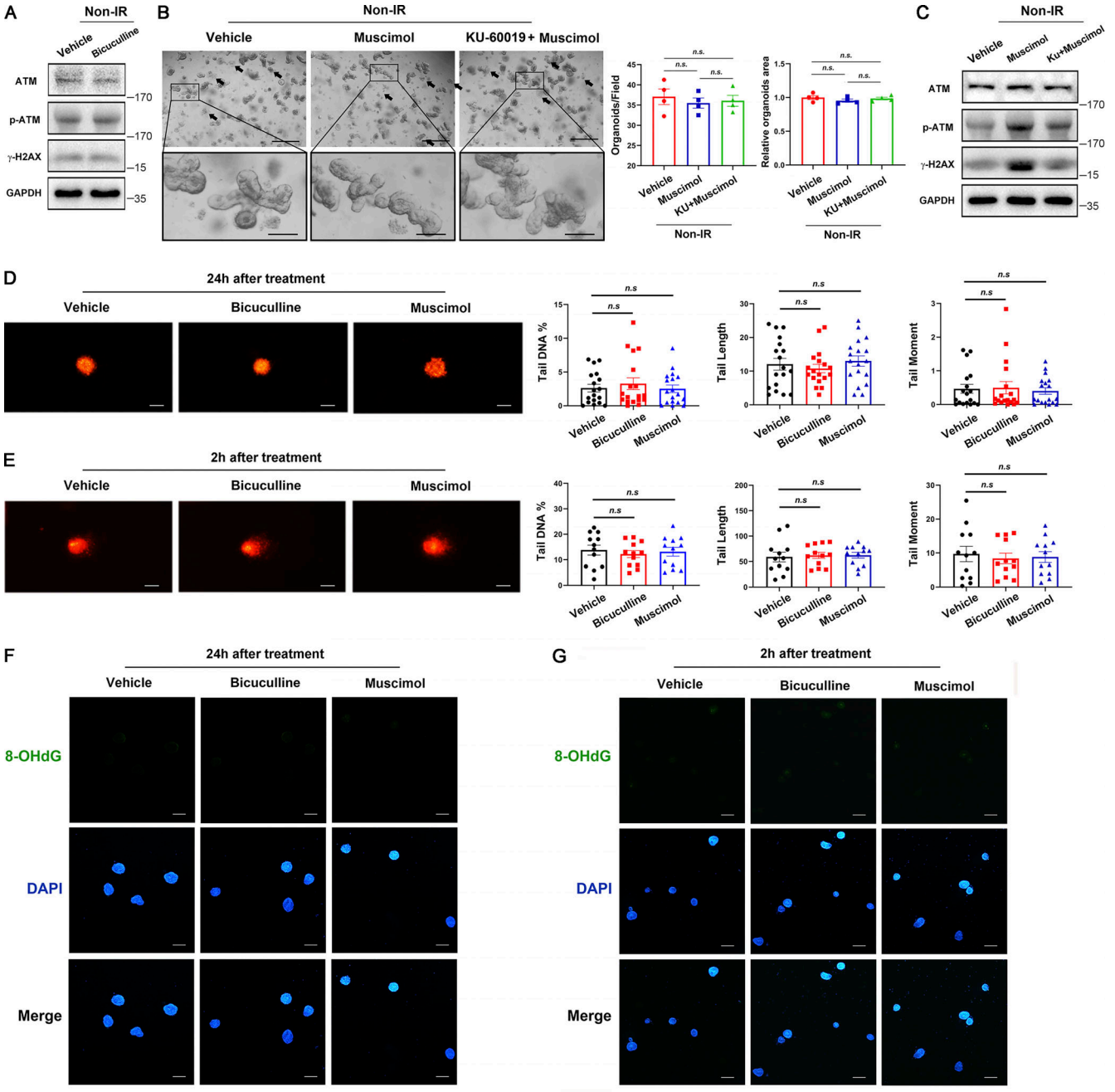

Figure S3. **Bicuculline or muscimol had no effect on ROS or DNA damage in organoids in the absence of 5-FU or irradiation treatment. (A)** Immunoblots of ATM, p-ATM, and γ-H2AX in the organoids after 2 h with or without bicuculline (1 μM) treatment. **(B)** Representative images of the organoids 2 d after vehicle, muscimol (1 μM), or KU60019 (1 μM) + muscimol (1 μM) treatment. Scale bar, 500 μm (upper) or 100 μm (bottom). Arrows indicate dead organoids. **(C)** Immunoblots of ATM, p-ATM, and γ-H2AX in the organoids 1.5 h after treatment as in B. **(D and E)** Representative images of the comet assay of individual cells isolated from the organoids 24 h (D) or 2 h (E) after indicated treatment. Scale bar, 25 μm. **(F and G)** Representative immunofluorescence images of 8-OHdG (green) staining of the organoids 24 h (F) or 2 h (G) after indicated treatment. Scale bar, 100 μm. In B, D, and E, values are means ± SEM. n.s., not significant (two-tailed Student's *t* test). Data are representative of two (D–G) or three (A–C) independent experiments. Source data are available for this figure: SourceData FS3.

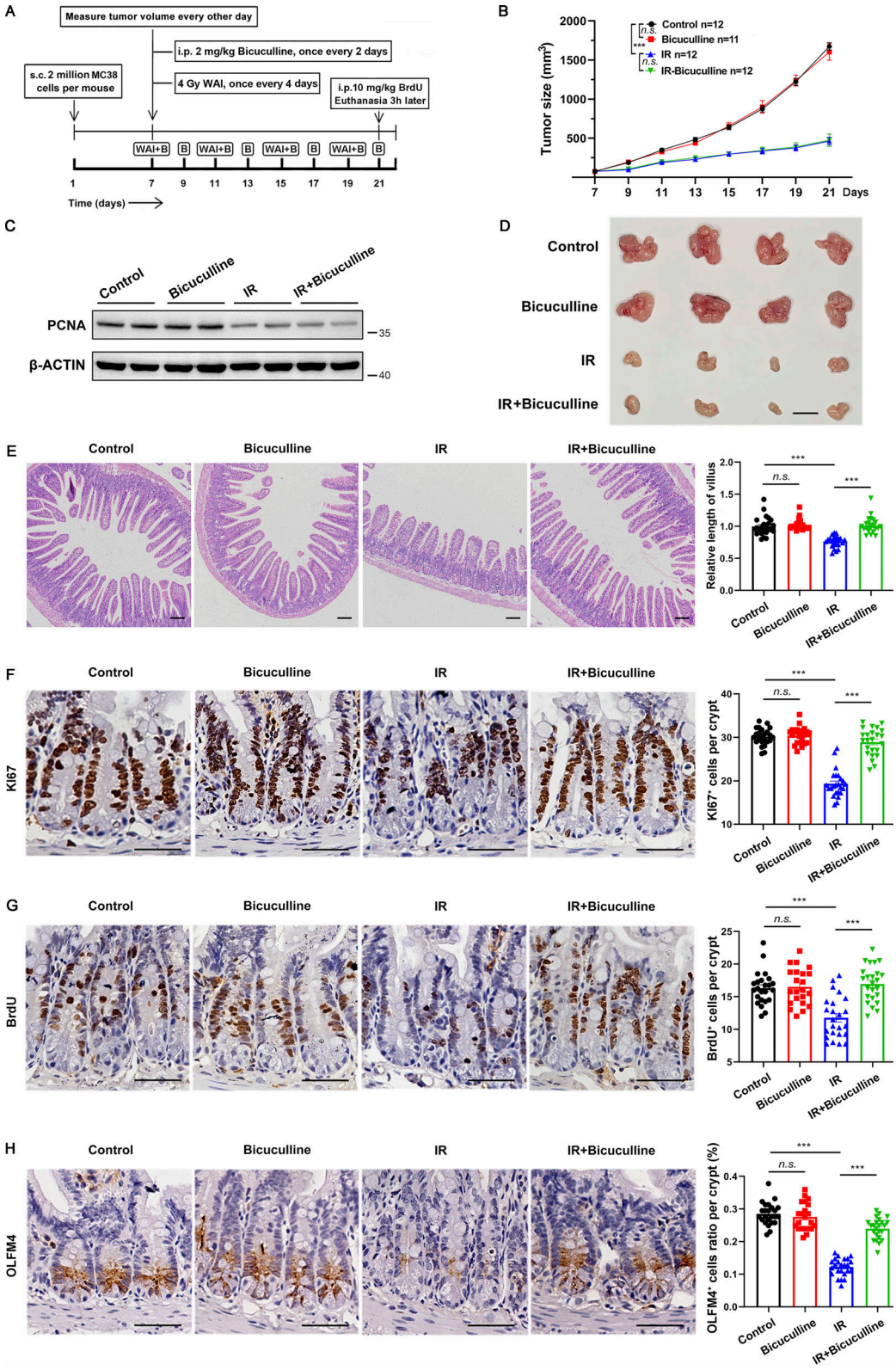

Figure S4. **Bicuculline protected the normal intestine of MC38 tumor-bearing mice from fractionated abdominal radiotherapy without affecting its antitumor activity. (A)** Schematic diagram of MC38 tumor-bearing mice exposed to fractionated abdominal irradiation. **(B)** Tumor sizes were measured every other day from days 7 to 21. **(C)** Immunoblot of PCNA expression in tumors from A at day 21. **(D)** Representative images of MC38 tumors at day 21. Scale bar, 1 cm. **(E)** Representative images of H&E staining of the jejunum tissues from mice treated as in A. Scale bar, 100 µm. **(F–H)** Representative images of KI67 (F), BrdU (G), and OLFM4 (H) staining of the jejunum tissues from mice treated as in A. Scale bar, 50 µm. In B, values are means ± SEM; *n* = indicated mice per group. ***, P < 0.001 (ANOVA). In E–H, values are means ± SEM; *n* = indicated mice per group. n.s., not significant; and ***, P < 0.001 (two-tailed Student's *t* test). Data are representative of at least two (B–H) independent experiments. Source data are available for this figure: SourceData FS4.

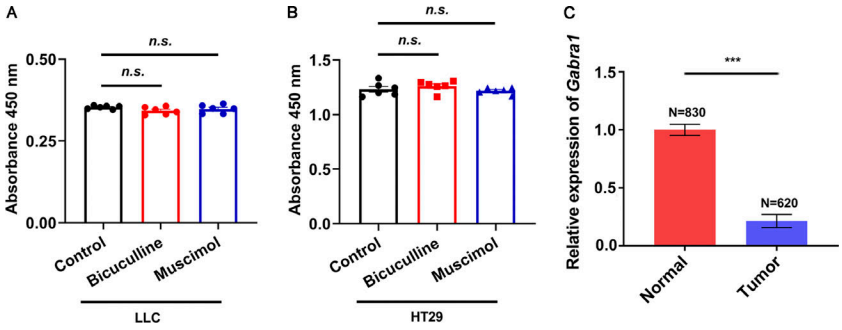

Figure S5. **Bicuculline or muscimol did not affect tumor cell line proliferation. (A and B)** CCK-8 cell proliferation assay analysis of LLC (A) and HT29 (B) proliferation after bicuculline (1 µM) or muscimol (1 µM) treatment. **(C)** The relative expression of *Gabra1* mRNA in colon adenocarcinoma tissues (n = 620) and normal colon tissues (n = 830) in TCGA and GTEx databases. Values are means ± SEM. n.s., not significant; and ***, P < 0.001 (two-tailed Student's t test). Data are representative of at least two (A and B) independent experiments.

Provided online are Table S1 and Table S2. Table S1 lists antibodies used in this study. Table S2 lists the primers used for RT-PCR analysis.